iScience

CellPress
OPEN ACCESS

Article

GSK3 inhibitor ameliorates steatosis through the modulation of mitochondrial dysfunction in hepatocytes of obese patients

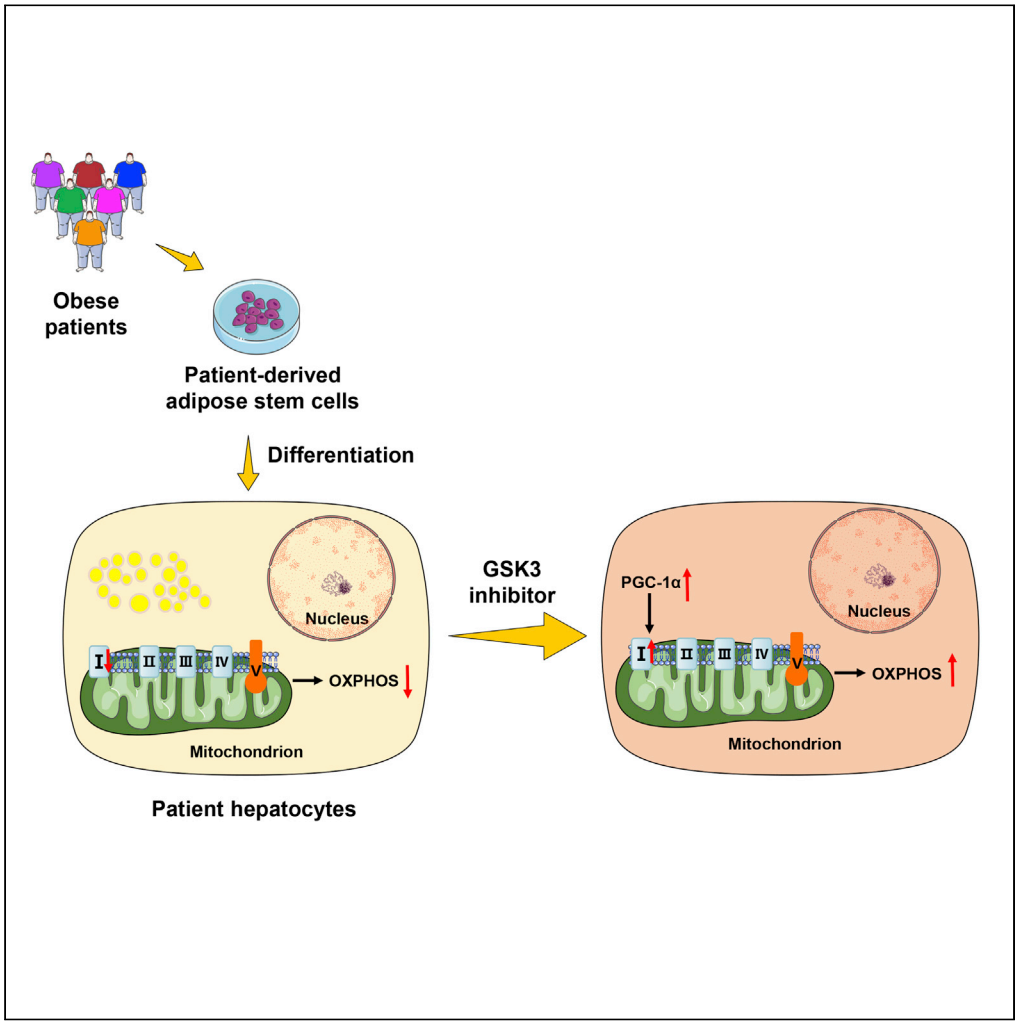

Yaqiong Li, Yi Lin, Xueya Han, ..., Xiaowu Huang, Rixing Bai, Haiyan Zhang

brx5168@163.com (R.B.)
culture@ccmu.edu.cn (H.Z.)

HIGHLIGHTS

Obese patients' adipose-stem-cell-derived hepatocytes reveal hepatic steatosis

Hepatic steatosis is accompanied the mitochondrial dysfunction

The mitochondrial dysfunction is governed by the low expression PGC-1α, TFAM, and NRF1

GSK3 inhibitor ameliorates hepatic steatosis via mitochondrial dysfunction modulation

Li et al., iScience *24*, 102149
March 19, 2021
https://doi.org/10.1016/j.isci.2021.102149

iScience

CellPress
OPEN ACCESS

Article

GSK3 inhibitor ameliorates steatosis through the modulation of mitochondrial dysfunction in hepatocytes of obese patients

Yaqiong Li,[1] Yi Lin,[2] Xueya Han,[1] Weihong Li,[1] Wenmao Yan,[2] Yuejiao Ma,[1] Xin Lu,[1] Xiaowu Huang,[3] Rixing Bai,[2,4,*] and Haiyan Zhang[1,4,5,*]

SUMMARY

Obesity is an important risk factor and a potential treatment target for hepatic steatosis. The maladaptation of hepatic mitochondrial flexibility plays a key role in the hepatic steatosis. Herein, we found that hepatocyte-like cells derived from human adipose stem cell of obese patients exhibited the characteristics of hepatic steatosis and accompanied with lower expression of the subunits of mitochondrial complex I and lower oxidative phosphorylation levels. The GSK3 inhibitor CHIR-99021 promoted the expression of NDUFB8, NDUFB9, the subunits of mitochondrial complex I, the basal oxygen consumption rate, and the fatty acid oxidation of the hepatocytes of obese patients by upregulating the expression of the transcription factor PGC-1α, TFAM, and NRF1 involved in mitochondrial biogenesis. Moreover, CHIR-99021 decreased the lipid droplets size and the triglyceride levels in hepatocytes of obese patients. The results demonstrate that GSK3 inhibition ameliorates hepatic steatosis by elevating the mitochondrial function in hepatocytes of obese patients.

INTRODUCTION

Fatty liver disease (FLD) has emerged as the most prevalent chronic liver disease and greatest risk factor for liver-related morbidity and mortality (Estes et al., 2018; Fan et al., 2017). Hepatic steatosis, which describes a range of conditions caused by triglyceride deposition within hepatocytes, is a major driver of FLD, which can progress to more advanced stages, including steatohepatitis, fibrosis, cirrhosis, and hepatocellular carcinoma (Engin, 2017; Friedman et al., 2018; Singh et al., 2015). Given that the worldwide increase in FLD prevalence parallels the evolution of the obesity epidemic, obesity is considered the most important risk factor and a potential target for the treatment of hepatic steatosis and FLD (Cusi, 2012; Eslam et al., 2018; Fan et al., 2017; Grohmann et al., 2018; Samuel and Shulman, 2018). Indeed, the high levels of fatty acids entering, high levels of triglyceride synthesis, and lower capacity of beta-oxidation in mitochondria lead to steatosis in the liver (Cusi, 2012; Engin, 2017). Notably, the continuous maladaptation of hepatic mitochondrial flexibility in obese individuals plays a key role in the pathogenesis of hepatic steatosis (Koliaki et al., 2015; Sunny et al., 2017). However, validation of predictive biomarkers of inadequate mitochondrial adaptation and response to therapy is lacking and is urgently needed. Moreover, an obese individual's susceptibility to substrate overload is highly variable, because of many different properties such as sedentary lifestyle, diet, intrauterine environment, and aging (Fan et al., 2017). Thus, understanding of the hepatic mitochondrial flexibilities and their maladaptation responses in hepatic steatosis will be helpful to offer new precision molecular targets for treatment of FLD and associated diseases.

Accumulating evidence indicates that human adipose stem cell (hASC)-derived hepatocyte-like cells (HLCs) offer an attractive tools for establishing an alternative therapy for liver dysfunction (Aurich et al., 2009; Banas et al., 2007; Hu et al., 2019; Li et al., 2014, 2018; Seo et al., 2005; Yuan et al., 2015). Recent studies showed that the environment or niche of obesity-related adipose tissue may have latent effects on immunophenotypic profile and adipogenic differentiation (Louwen et al., 2018; Oñate et al., 2013; Pachon-Pena et al., 2016), immune properties (Serena et al., 2016, 2017), and primary cilia function (Ritter et al., 2018). However, evidence showing the hepatic differentiation capability of obese patient hASCs is currently lacking.

[1]Department of Cell Biology, School of Basic Medical Science, Capital Medical University, Beijing, 100069, China

[2]Department of General Surgery, Beijing Tian Tan Hospital, Capital Medical University, Beijing, 100070, China

[3]Fu Xing Hospital, Capital Medical University, Beijing, 100038, China

[4]These authors contributed equally

[5]Lead contact

*Correspondence: brx5168@163.com (R.B.), culture@ccmu.edu.cn (H.Z.)

https://doi.org/10.1016/j.isci.2021.102149

Table 1. Characteristics of the patients

	Lean (n = 8)	Obese (n = 18)	p Value
Age (years)	35.88 ± 5.239	32.67 ± 1.464	0.4373
Gender (male/female)	8 (2/6)	18 (10/8)	/
Body mass index (kg/m^2)	22.21 ± 0.8169	42.44 ± 2.015	<0.0001
Glucose (mmol/L)	4.715 ± 0.2111	7.314 ± 0.7909	0.0417
Fasting serum insulin (uU/mL)	/	20.24 ± 2.333	/
HOMA-IR	/	2.690 ± 0.3271	/
Triglyceride (mmol/L)	1.104 ± 0.1726	2.894 ± 0.8006	0.1551
Total cholesterol (mmol/L)	4.429 ± 0.2426	4.536 ± 0.2674	0.8073
HDL-cholesterol (mmol/L)	1.245 ± 0.07741	0.9650 ± 0.04861	0.0045
LDL-cholesterol (mmol/L)	2.644 ± 0.1993	2.810 ± 0.2761	0.7079
HbA1c (%)	/	7.667 ± 0.4658	/

HOMA-IR, homeostasis model assessment of insulin resistance; HDL, high-density lipoprotein; LDL, low-density lipoprotein. Data are expressed as the means ± SEM.

Here, we found that hASC-HLCs from obese subjects exhibited the characterization of hepatic steatosis associated with maladaptation of mitochondrial oxidative activity, as indicated by lower expression of the subunits of mitochondrial complex I, the basal oxygen consumption rate (OCR), and fatty acid oxidation. Moreover, we found that the GSK3 pharmacological inhibitor CHIR-99021 modified the mitochondrial dysfunction of the hASC-HLCs of obese patients by upregulating the expression of the transcription factor PGC-1α, TFAM, and NRF1 involved in mitochondrial biogenesis and respiratory function. Meantime, CHIR-99021 treatment ameliorates hepatic steatosis in hASC-HLCs of obese patients.

RESULTS

hASCs from obese patients possess the potential to differentiate into hepatocytes

We initially isolated and evaluated the phenotypes of the ASCs from the visceral adipose tissue of eighteen obese patients undergoing bariatric surgery and eight lean control donors undergoing selective caesarean section at term (Table 1). The majority of the cells from the both lean control and obese donors exhibited a typical uniform spindle-shaped appearance of morphogenic fibroblasts at the 6th passage (Figure S1). The cultured hASCs from both lean controls and obese donors exhibited the same expression of these typical surface markers, with more than 96% of the samples positive for CD73, CD90, and CD105 and almost all the samples negative for CD34 (Figure S2). The data confirmed that the hASCs from the obese patients maintained a similar morphology and phenotype as those from the control donors.

To assess whether hASCs derived from obese patients possess the potential to differentiate into HLCs, hASCs from lean control donors and obese donors were differentiated using a three-stage differentiation protocol as previously described (Li et al., 2014). The properties of the differentiated cells in the two groups were analyzed on day 5, day 10, and day 20 during the process of hepatic differentiation of hASCs. Immunofluorescence staining data verified that, on day 5, the cells in the two groups were positive for GATA-binding protein 4 (GATA4) (Figure 1A), which is a marker of definitive endoderm cells; on day 10, the cells were positive for α-fetoprotein (AFP) (Figure 1B), which is a marker of hepatic progenitor cells; and on day 20, they were positive for glutathione S-transferase alpha 2 (GSTA2), which is a marker of hepatocytes (Figure 1C). These data indicated that hASCs derived from obese donors can be differentiated into HLCs that exhibit hepatocyte-specific proteins by mimicking liver embryogenesis and maturation induction. Therefore, we named the HLCs from the two groups: lean HLCs (HLCs derived from ASCs of lean donors) and obese HLCs (HLCs derived from ASCs of obese patients).

To further characterize the obese HLCs, typical hepatic markers were determined using real-time RT-PCR. Quantitative comparisons of gene expression revealed that the expression of ATP-binding cassette, subfamily C (CFTR/MRP), member 2 (ABCC2), and phosphoenolpyruvate carboxykinase 2 (PCK2) in the cells of the two groups did not differ. However, the mRNA levels of hepatocyte nuclear factor 4 alpha (HNF4α), albumin (ALB), cytochrome P450 family 3 subfamily A member 4 (CYP3A4), and carbamoyl-phosphate synthase 1 (CPS1) in the cells derived from obese donors were relatively lower than were those in the cells

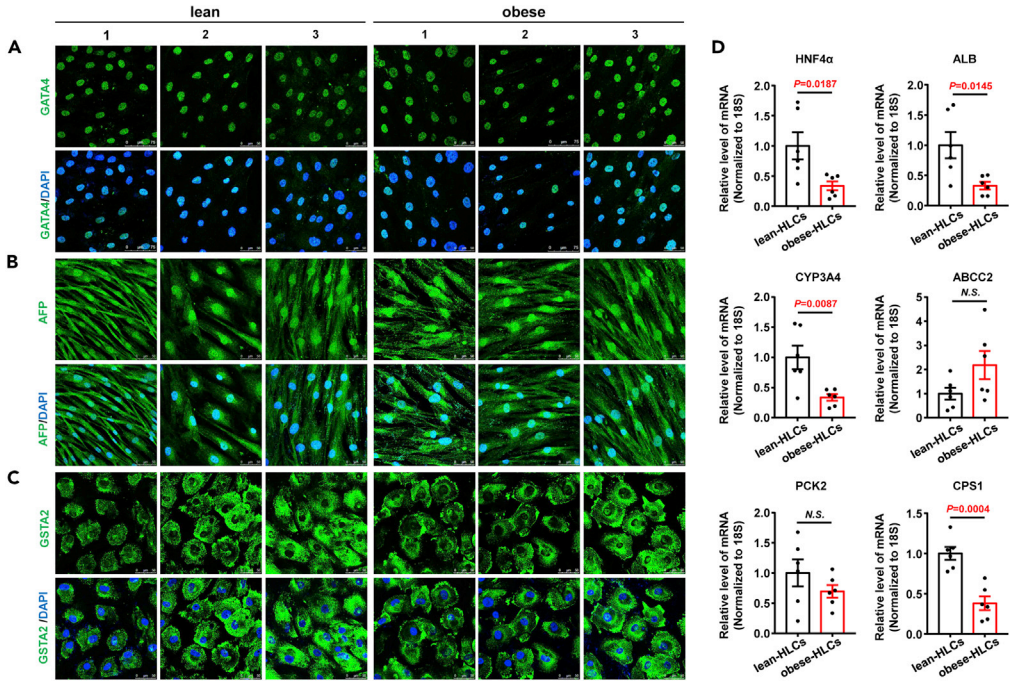

Figure 1. hASCs from obese donors possess the potential to differentiate into hepatocyte-like cells

Immunofluorescence analysis of differentiated hASCs in the two groups was used to determine the expression of GATA4 (A), AFP (B), and GSTA2 (C). Scale bars, 50 μm and 75 μm. Obese, obese donor; lean, lean donor; 1, 2, and 3 represent donor 1, donor 2, and donor 3, respectively. (D) Relative mRNA levels of hepatic functional markers, namely, HNF4α, ALB, CYP3A4, ABCC2, PCK2, and CPS1, in the lean HLCs and obese HLCs were determined by real-time RT-PCR. n = 6 different donors per group. Significance compared with the lean HLCs, as analyzed by unpaired two-tailed Student's t test. Data are presented as the means ± SEM. *N.S.*, not significant. hASCs, human adipose stem cells; lean HLCs, hepatocyte-like cells derived from adipose stem cell of lean donors; obese HLCs, hepatocyte-like cells derived from adipose stem cell of obese patients; GATA4, GATA-binding protein 4; AFP, α-fetoprotein; GSTA2, glutathione S-transferase alpha 2; HNF4α, hepatocyte nuclear factor 4 alpha; ALB, albumin; CYP3A4, cytochrome P450 family 3 subfamily A member 4; ABCC2, ATP-binding cassette, sub-family C (CFTR/MRP), member 2; PCK2, phosphoenolpyruvate carboxykinase 2; CPS1, carbamoyl-phosphate synthase 1. See also Figures S1–S3.

derived from the control lean donors (Figures 1D and S3). These data indicated differential gene expression of the obese HLCs and lean HLCs.

Differential gene expression in the lean HLCs and obese HLCs

To obtain an initial perspective on global gene expression changes, RNA sequencing was performed to compare the gene expression in the lean HLCs and obese HLCs. The results revealed that 48 genes were significantly upregulated and 49 were significantly downregulated in the obese HLCs (Figure 2A). A functional gene annotation analysis of these differentially expressed genes was performed according to gene subset to explore the functions of these regulated genes in the lean HLCs and obese HLCs. Analysis of the significantly upregulated genes in the obese HLCs led to the identification of functional groups, such as "bleb assembly," "ossification," "cellular response to extracellular stimulus", "cytolysis," "cell morphogenesis," and "glycosaminoglycan catabolic process" (Figure 2B). Analysis of the significantly downregulated genes found in the obese HLCs led to the identification of functional groups, such as "renal absorption," "regulation of cell proliferation," "positive regulation of protein phosphorylation," "cell chemotaxis," "blood coagulation," "positive regulation of peptidyl-tyrosine phosphorylation," "positive regulation of leukocyte chemotaxis," and "positive regulation of reactive oxygen species metabolic process" (Figure 2C).

GSEA analyses revealed that the pathways related to "glycerolipid metabolism (HSA00561)," "steroid biosynthesis (HSA00100)," "sphingolipid signaling (HSA04071)," "cholesterol biosynthetic process (GO0006695)," and "the positive regulation of interleukin 6 production (GO0032755)" were significantly

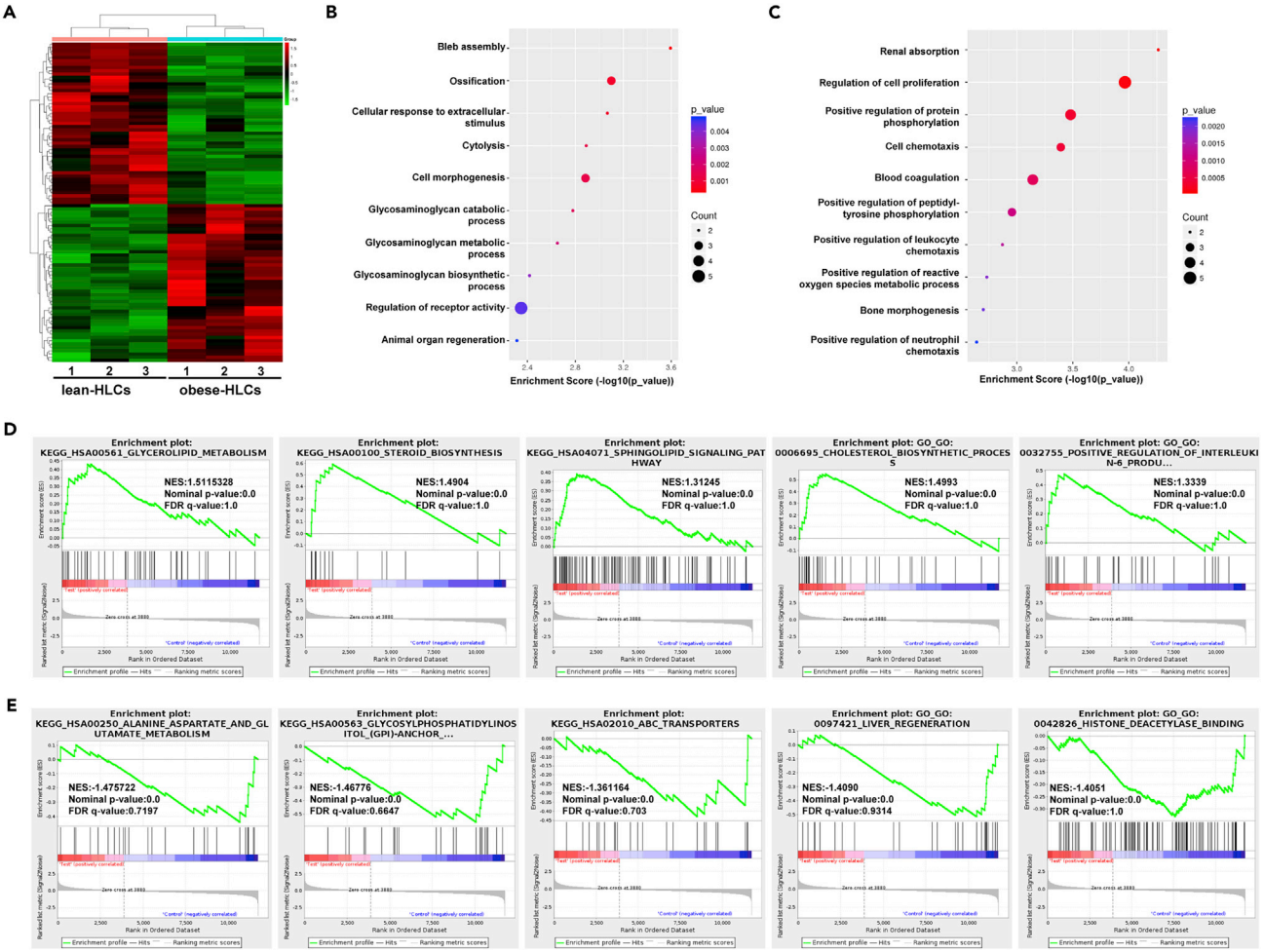

Figure 2. Comparative analysis of differentially expressed genes in the lean HLCs and obese HLCs based on RNA sequencing

(A) Heatmap generated by the common genes shared between the two groups based on different gene subsets using MeV v4.8 (http://www.tm4.org/mev/). In the heatmap, high expression is depicted in red, and low expression is depicted in green. The columns are log10 plots of the normalized intensity of triplicate samples in each group.

(B) Results of GO analysis of biological process of the differentially expressed upregulated genes in the obese HLCs.

(C) Results of GO analysis for the biological process of the differentially expressed downregulated genes in the obese HLCs.

(D) GSEA for the KEGG pathways and GO analysis of the differentially expressed upregulated genes in the obese HLCs.

(E) GSEA for KEGG pathways and GO analysis of the differentially expressed downregulated genes in the obese HLCs. n = 3 different donors per group. Lean HLCs, hepatocyte-like cells derived from adipose stem cell of lean donors; obese HLCs, hepatocyte-like cells derived from adipose stem cell of obese patients; GO, gene ontology; GSEA, gene set enrichment analysis; KEGG, Kyoto Encyclopedia of Genes and Genomes.

See also Figures S4–S6.

upregulated (Figure 2D). Genes involved in these pathways are listed in the Supplemental information, Figure S4. However, the pathways related to "alanine aspartate and glutamate metabolism (HSA00250)," "glycosylphosphatidylinositol anchor (00563)," "ABC transporters (HSA02010)," "liver regeneration (GO0097421)," and "histone deacetylase binding (GO0042826)" were significantly downregulated (Figure 2E). Genes involved in these pathways are listed in the Supplemental information, Figure S5.

To validate the accuracy of the gene indexes calculated from RNA sequencing, five upregulated expression genes, including glycerol kinase (GK) in the glycerolipid metabolism pathway, sterol-C5-desaturase (SC5D) in the steroid biosynthesis pathway, Rac family small GTPase 3 (RAC3) in the sphingolipid signaling pathway, insulin-induced gene 1 (INSIG1) in the cholesterol biosynthetic process, and lipopolysaccharide binding protein (LBP) in the positive regulation of interleukin-6 production were confirmed by real-time RT-PCR (Figure S6A). In addition, five downregulated genes, including glutamine-fructose-6-phosphate

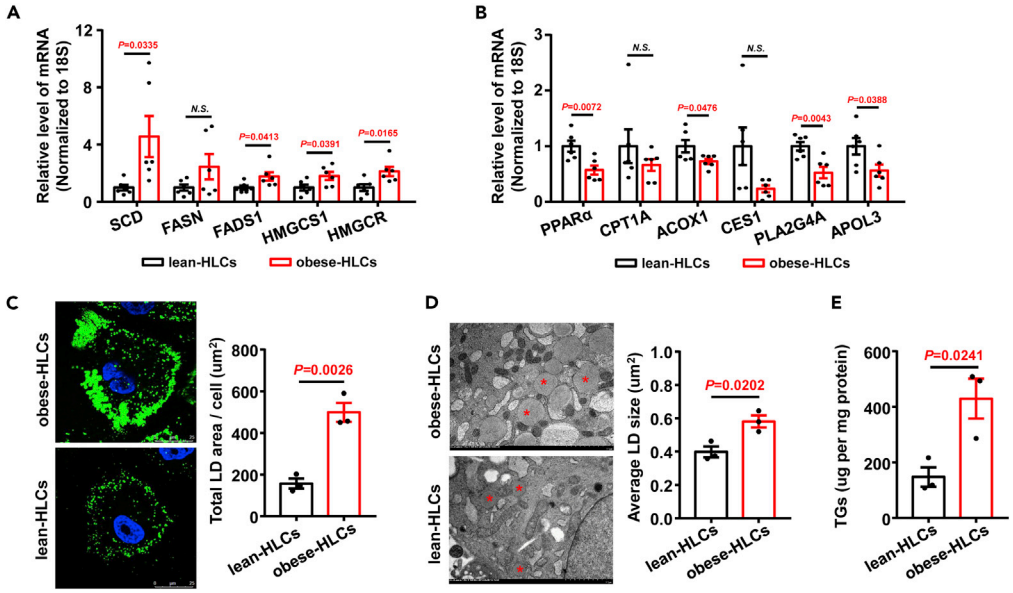

Figure 3. Comparisons of the lipid metabolic properties in the lean HLCs and obese HLCs

(A and B) Relative mRNA levels of lipid-metabolism-related genes in the lean HLCs and obese HLCs were determined by real-time RT-PCR. (A) Lipid synthesis genes, namely, SCD, FASN, FADS1, HMGCS1, and HMGCR; (B) genes related to the fatty acid β-oxidation pathway, namely, PPARα, CPT1A, ACOX1, CES1, PLA2G4A, and APOL3. n = 6 different donors per group.

(C) LDs in the lean HLCs and obese HLCs were determined by HCS LipidTOX green neutral lipid staining. Scale bars, 25 μm. Total LD area in each cell was analyzed using ImageJ software. n = 3 different donors per group; the number of cells was 100 in each donor respectively.

(D) The size of LD in the lean HLCs and obese HLCs was determined using TEM. The red asterisk indicates an LD. Scale bars, 2 μm. The average LD size in the cells was determined using ImageJ software. n = 3 different donors per group.

(E) TG levels of HLCs from lean donors and obese donors were determined by using a triglyceride assay kit. Significance compared with the lean HLCs, as analyzed by unpaired two-tailed Student's t test. *N.S.*, not significant. Data are presented as the means ± SEM. n = 3 different donors per group. Lean HLCs, hepatocyte-like cells derived from adipose stem cell of lean donors; obese HLCs, hepatocyte-like cells derived from adipose stem cell of obese patients; SCD, stearoyl-CoA desaturase; FASN, fatty acid synthase; FADS1, fatty acid desaturase 1; HMGCS1, 3-hydroxy-3-methylglutaryl-CoA synthase 1; HMGCR, 3-hydroxy-3-methylglutaryl-CoA reductase; PPARα, peroxisome-proliferator-activated receptor alpha; CPT1A, carnitine palmitoyltransferase 1A; ACOX1, acyl-CoA oxidase 1; CES1, carboxylesterase 1; PLA2G4A, phospholipase A2 group IVA; APOL3, apolipoprotein L3; LDs, lipid droplets; TEM, transmission electron microscopy.

See also Figures S7 and S8.

transaminase 2 (GFPT2) in the alanine aspartate and glutamate metabolism pathways, post-GPI attachment to protein inositol deacylase 1 (PGAP1) in the glycosylphosphatidylinositol anchor pathway, transporter 2, ATP-binding cassette subfamily B member (TAP2) in the ABC transporter pathway, proliferating cell nuclear antigen (PCNA) in liver regeneration, and DNA topoisomerase II beta (TOP2B) in histone deacetylase binding, were also confirmed by real-time RT-PCR (Figure S6B). These data suggest that obese HLCs exhibit the characteristics of abnormally elevated lipid metabolism and reduced liver regeneration compared with the metabolism and regeneration in the lean HLCs.

Obese HLCs exhibit the characteristics of hepatic steatosis

Obesity-related hepatic steatosis represents imbalances of the processes that maintain the normal homeostasis of lipid metabolism in the hepatocyte can lead to hepatic dysfunction (Gluchowski et al., 2017). To investigate whether obese HLCs exhibit the characteristics of hepatic steatosis, the expression levels of genes involved in lipid synthesis and lipolysis in the lean HLCs and obese HLCs were quantitatively compared using real-time RT-PCR. As shown in Figure 3, the results indicated that genes related to fatty acid synthesis, including stearoyl-CoA desaturase (SCD) and fatty acid desaturase 1 (FADS1), and genes involved in the rate-limiting enzyme step of cholesterol synthesis, including 3-hydroxy-3-methylglutaryl-CoA synthase 1 (HMGCS1) and 3-hydroxy-3-methylglutaryl-CoA reductase (HMGCR), were significantly

upregulated in the obese HLCs (Figure 3A). Genes related to the fatty acid beta-oxidation pathway, such as peroxisome proliferator-activated receptor alpha (PPARα), acyl-CoA oxidase 1 (ACOX1), phospholipase A2 group IVA (PLA2G4A), and apolipoprotein L3 (APOL3), were significantly downregulated in the obese HLCs (Figure 3B) compared with the levels in the lean HLCs. Fatty acid synthase (FASN), which is related to fatty acid synthesis, carboxylesterase 1 (CES1), which participate in hepatic lipid metabolism, and carnitine palmitoyltransferase 1A (CPT1A) in the fatty acid beta-oxidation pathway were not significantly different in the obese HLCs and the lean HLCs (Figure 3A and 3B).

The cytoplasmic lipid droplets (LDs) are lipid storage organelles in hepatocytes; the aberrant accumulation of LDs is the hallmark of steatosis, a key pathological feature of obesity, FLD, and metabolic syndrome (Gluchowski et al., 2017). To demonstrate changes in lipid accumulation, neutral lipids in the HLCs were quantitatively compared using HCS LipidTOX green neutral lipid stain. The results revealed that LDs were present both in the lean HLCs and in the obese HLCs. Quantitative analysis of the total area of LDs in the cells derived from three lean donors and obese donors revealed that the total area of LDs was significantly higher in the obese HLCs compared with that in the lean HLCs (Figures 3C and S7A). TEM analysis also demonstrated that the sizes of LDs in the obese HLCs were significantly larger than those in the lean HLCs (Figures 3D and S7B).

Free fatty acids (FAs) are taken up by hepatocytes and converted into triglycerides (TGs) for storage with cholesterol in LDs or imported to mitochondria for β-oxidation. TG levels were quantitatively compared in the lean HLCs and obese HLCs. Consistent with the increased LDs areas, the TG levels in the obese HLCs were higher than the lean HLCs (Figure 3E). By visualizing FAs in live cells, the labeled FA in LDs were accumulated in the obese HLCs than those in the lean HLCs (Figures S8A and S8B). However, the labeled FA localized with mitochondria were decreased in the obese HLCs than those in the lean HLCs (Figures S8C and S8D). These data suggest that the metabolic imbalances between the synthesis or storage and degradation of lipid triggered increased TG and LD accumulation in obese HLCs. These characteristics are consistent with those of hepatocyte steatosis.

Obese HLCs exhibit altered mitochondrial structure and oxidative phosphorylation function

Recent evidence suggests that continuous maladaptation of mitochondrial energetics, gene expression, morphology, and content plays a key role in the pathogenesis of simple steatosis (Sunny et al., 2017). To investigate changes in the mitochondria in the obese HLCs, the mitochondrial structure and function were first evaluated. The results revealed that the mitochondrial mass in the obese HLCs was significantly lower than that in the lean HLCs (Figures 4A and S9A). TEM analysis also demonstrated that the mitochondria in the obese HLCs contained immature mitochondria with a globular shape and poorly developed cristae indicative of a less-active mitochondrial state, whereas the lean HLCs possessed a complex morphology with developed cristae, a dense matrix, and an elongated appearance (Figures 4B and S9B). The mtDNA content in the obese HLCs was significantly decreased compared with that in the lean HLCs (Figure 4C). The mitochondrial membrane potential in the obese HLCs was also significantly lower than that in the lean HLCs (Figures 4D and S10).

Adenosine triphosphate (ATP) production rates measured using Agilent Seahorse XF technology demonstrated that the proportion of the mitochondrial oxidative phosphorylation pathway contributing to the ATP (mitoATP) production rate in the lean-HLCs was ~37%, whereas the proportional mitoATP production rate in the obese HLCs was only ~21% ± 6% (Figure 4E). The proportion of the basal OCR and ECAR in the obese HLCs was significantly lower than that in the lean HLCs (Figure 4F).

Mitochondrial superoxide is generated as a by-product of oxidative phosphorylation. The production of ROS derived from mitochondria was determined using MitoSOX red mitochondrial superoxide indicator, a fluorogenic dye for the highly selective detection of superoxide in the mitochondria of live cells. The results revealed that the source of mitochondrial ROS in the obese HLCs was lower than that in the lean HLCs (Figure 4G). These data indicated that the obese HLCs exhibit an altered mitochondrial structure and lower oxidative phosphorylation activities than were exhibited by the lean HLC controls.

Obese HLCs exhibit lower expression of the subunits of mitochondrial complex I

The mitochondrial respiratory chain complexes respond by converting energy produced during metabolism into synthesized ATP during oxidative phosphorylation. To investigate the expression of the mitochondrial

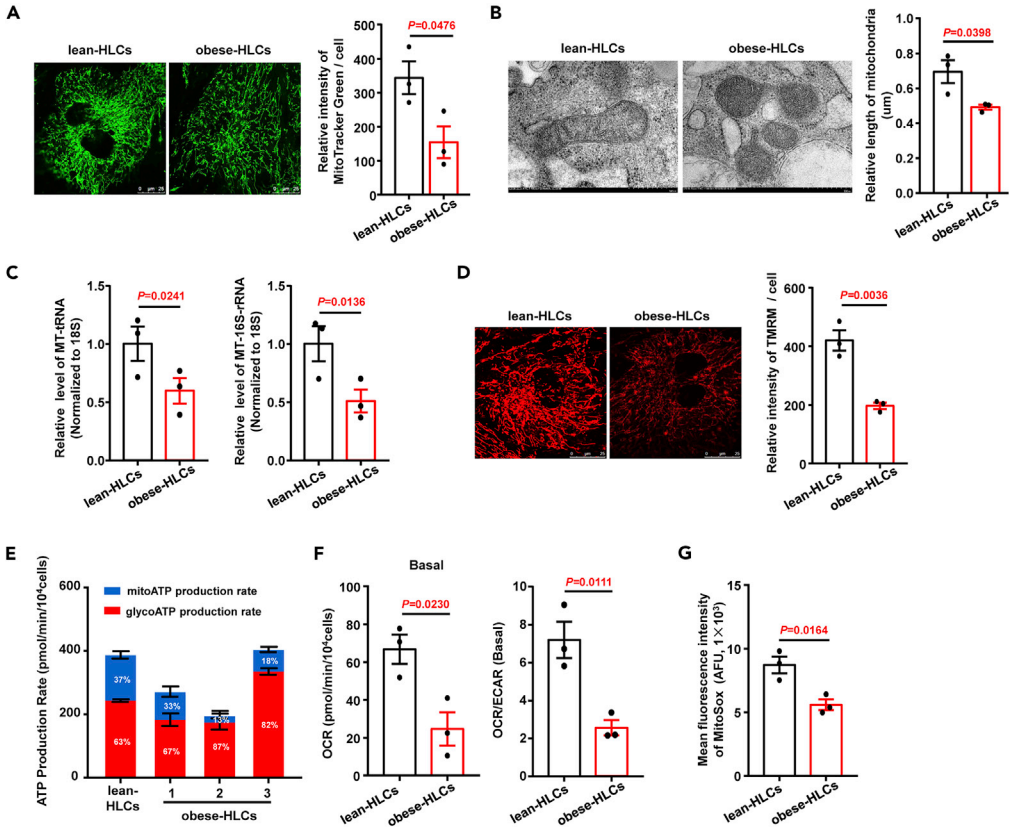

Figure 4. Comparisons of the mitochondrial mass and oxidative phosphorylated activity levels in the lean HLCs and obese HLCs

(A) Mitochondrial mass in the lean HLCs and obese HLCs was determined by MitoTracker Green FM. Scale bars, 25 μm. The fluorescence intensity of MitoTracker Green in each cell was analyzed using ImageJ software. n = 3 different donors per group; the number of cells was 100 in each donor respectively.

(B) Mitochondrial morphology in the lean HLCs and obese HLCs was determined by TEM. Scale bars, 500 nm. The relative length of mitochondria in the cells was determined using ImageJ software. n = 3 different donors per group.

(C) Relative mitochondrial DNA content (measured as mitochondrial tRNA and 16S-rRNA) in the lean HLCs and obese HLCs was determined by real-time PCR. n = 3 different donors per group.

(D) Mitochondrial potential in the lean HLCs and obese HLCs was determined by TMRM. Scale bars, 25 μm. The fluorescence intensity of TMRM in each cell was analyzed using ImageJ software. n = 3 different donors per group; the number of cells was 100 in each donor respectively.

(E) ATP production rate as determined using the Seahorse XF Real-Time ATP rate assay and the mitoATP and glycoATP production rates in the lean HLCs and obese HLCs were calculated. Obese HLCs, n = 3 different donors.

(F) The basal OCR and OCR/ECAR were calculated in the lean HLCs and obese HLCs. n = 3 different donors per group.

(G) The production levels of mitochondrial ROS in the lean HLCs and obese HLCs, as labeled by MitoSox and immediately measured using flow cytometry. n = 3 different donors per group. Significance compared with the lean HLCs, as analyzed by unpaired two-tailed Student's t test. Data are presented as the means ± SEM. Lean HLCs, hepatocyte-like cells derived from adipose stem cell of lean donors; obese HLCs, hepatocyte-like cells derived from adipose stem cell of obese patients; OCR, oxygen consumption rate; ECAR, extracellular acidification rate; mitoATP, mitochondrial oxidative phosphorylation pathway contributing to the ATP; glycoATP, glycolysis pathway contributing to the ATP; ROS, reactive oxygen species; TEM, transmission electron microscopy.

See also Figures S9 and S10.

electron transport chain complex in the obese HLCs, the mRNA levels of the electron transport chain complex components were analyzed using RNA sequencing according to gene subset. Interestingly, the significantly downregulated genes were focused on the accessory or supernumerary subunits of respiratory chain complex I (NADH:ubiquinone oxidoreductase), which included NADH:ubiquinone oxidoreductase subunit (NDUF)A8, NDUFA9, NDUFB6, NDUFB8, NDUFB9, and NDUFS8 (Figure S11). Real-time RT-PCR analysis showed that the expression of NDUFA8, NDUFB6, NDUFB8, NDUFB9, and NDUFS8 was significantly decreased in the obese

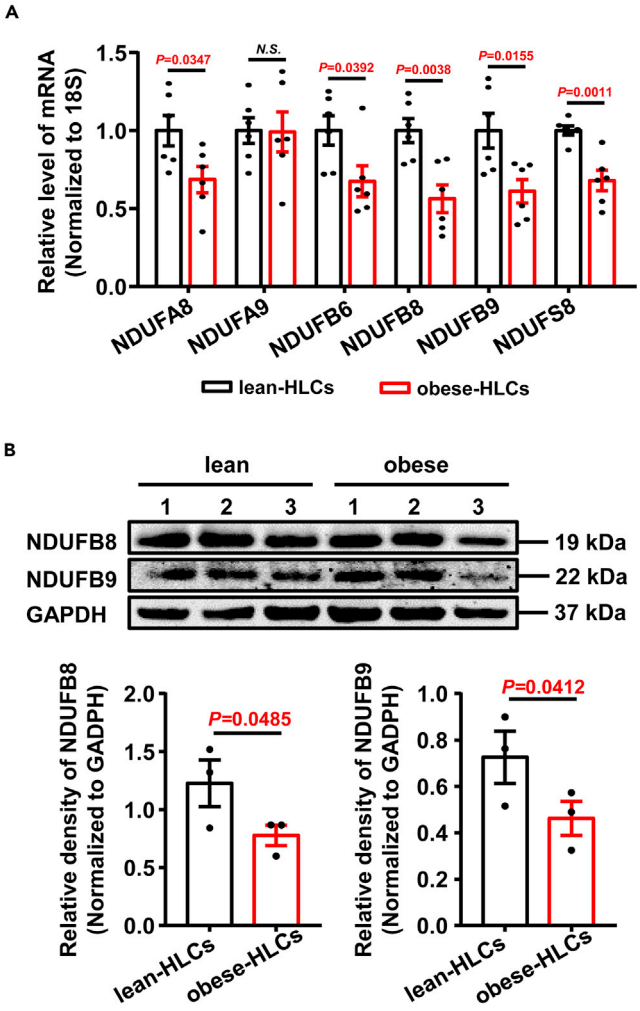

Figure 5. Comparative analysis of the expression of the complex I subunits of mitochondria in the lean HLCs and obese HLCs

(A) Relative mRNA levels of NDUFB6, NDUFA8, NDUFB8, NDUFS8, NDUFA9, and NDUFB9 in the lean HLCs and obese HLCs were determined by real-time RT-PCR. n = 6 different donors per group.

(B) Protein levels of NDUFB8 and NDUFB9 in the lean HLCs and obese HLCs were determined by western blotting. Relative band densities of NDUFB8 and NDUFB9 were normalized to that of GAPDH and analyzed using ImageJ software. n = 3 different donors per group. Significance compared with the lean HLCs, as analyzed by unpaired two-tailed Student's t test. Data are presented as the means ± SEM. *N.S.*, not significant. Lean HLCs, hepatocyte-like cells derived from adipose stem cell of lean donors; obese HLCs, hepatocyte-like cells derived from adipose stem cell of obese patients; GAPDH, glyceraldehyde-3-phosphate dehydrogenase; NDUFB6, NADH: ubiquinone oxidoreductase subunit B6; NDUFA8, NADH: ubiquinone oxidoreductase subunit A8; NDUFB8, NADH: ubiquinone oxidoreductase subunit B8; NDUFS8, NADH: ubiquinone oxidoreductase subunit S8; NDUFA9, NADH: ubiquinone oxidoreductase subunit A9; NDUFB9, NADH: ubiquinone oxidoreductase subunit B9.

See also Figure S11.

HLCs compared with the levels in the lean HLCs (Figure 5A). Western blot analysis confirmed that the protein levels of NDUFB8 and NDUFB9 were significantly decreased in the obese HLCs compared with their levels in the lean HLCs (Figure 5B). These data suggested that the lower expression of the subunits of mitochondrial complex I may be attributed to lower oxidative phosphorylation activities in the obese HLCs.

CHIR-99021 promotes mitochondrial remodeling in the obese HLCs

Previously, we found that a pharmacological inhibitor of glycogen synthase kinase-3 (GSK-3), CHIR-99021, promoted mitochondrial remodeling and oxidative phosphorylation activity during definitive endodermal

differentiation of hASCs by upregulating the expression of transcription factors, involved in mitochondrial biogenesis (Ma et al., 2019). To assess the effect of CHIR-99021 on remodeling in the obese HLCs, the obese HLCs were treated with 2 μM CHIR-99021 or vehicle control (DMSO) for 24 h. The mitochondrial contents and function in the obese HLCs were determined in the CHIR-99021-treated obese HLCs and compared with their expression in the vehicle-control-treated obese HLCs.

The results revealed that the mitochondrial contents including mitochondrial mass, the mtDNA content, and the protein levels of NDUFB8 and NDUFB9 were significantly increased in the CHIR-99021-treated obese HLCs compared with the levels in the vehicle-control-treated obese HLCs (Figures 6A–6C and S12). The mitochondrial mass and the protein levels of NDUFB8 and NDUFB9 were also significantly increased in the CHIR-99021-treated lean HLCs compared with the levels in the vehicle-control-treated lean HLCs (Figure S13).

The mitochondrial membrane potential and oxidative phosphorylation activities, which include the level of basal OCR values and ATP production, were significantly increased in the CHIR-99021-treated obese HLCs compared with that in the vehicle-control-treated obese cells (Figures 6D, 6E, and S14). The mitochondrial membrane potential and oxidative phosphorylation activities were also significantly increased in the CHIR-99021-treated lean HLCs compared with the levels in the vehicle-control-treated lean HLCs (Figure S15).

Mitochondria represent the primary site for fatty acid (FA) β-oxidation where FAs are enzymatically broken down to sustain cellular lipid dynamic regulation (Rambold et al., 2015). Using a pulse-chase labeling method to visualize movement of FAs in live cells, we demonstrate that CHIR-99021 promote the FAs flux into mitochondria in the obese HLCs (Figures 6F and S16). The protein levels of carnitine palmitoyl transferase 1 A (CPT1A), which allows the entry of FAs into mitochondria, were significantly increased in the CHIR-99021-treated obese HLCs compared with the levels in the vehicle-control-treated obese HLCs (Figures 6G and S17). These results suggest that CHIR-99021 may promote mitochondrial structural and functional remodeling in the obese HLCs.

CHIR-99021 upregulated the expression of transcription factors involved in mitochondrial biogenesis

In an attempt to understand the mechanism by which CHIR-99021 induces mitochondrial remodeling, we next examined the expression of transcription factors, including peroxisome proliferator-activated receptor gamma (PPARγ) coactivator-1α (PGC-1α), the master regulator of mitochondrial biogenesis and oxidative phosphorylation activity; mitochondrial transcription factor A (TFAM), a direct regulator of mitochondrial DNA replication and/or transcription; and nuclear respiratory factor 1 (NRF1), which controls all ten nucleus-encoded cytochrome oxidase subunits in the lean HLCs and obese HLCs. Real-time RT-PCR analyses showed that the mRNA levels of PGC-1α, TFAM, and NRF1 in the obese HLCs were significantly lower than those in the lean HLCs (Figure 7A). Western blotting analyses showed that the protein level of PGC-1α in the obese HLCs was lower than that in the lean HLCs (Figure 7B). Immunocytochemistry analyses showed that the relative fluorescence intensity for TFAM and NRF1 in the obese HLCs was also lower than it was in the lean HLCs (Figures 7C, 7D and S18).

Furthermore, the mRNA levels of PGC-1α, TFAM, and NRF1 in the CHIR-99021-treated obese HLCs were significantly increased compared with those in the vehicle-control-treated cells (Figure 7E). Western blot analyses showed that the protein levels of PGC-1α in CHIR-99021-treated obese HLCs were significantly increased compared with those of the vehicle-control-treated cells, but not in lean HLCs (Figures 7F and S19). Immunocytochemistry analyses showed that the relative fluorescence intensities of NRF1 and TFAM were significantly increased in the CHIR-99021-treated obese HLCs or CHIR-99021-treated lean HLCs compared with those of the vehicle-control-treated cells (Figures 7G, 7H, and S20). The changes of protein levels of TFAM between the CHIR-99021-treated HLCs and the vehicle-control-treated cells had inter-individual variability (Figure S20). These findings indicated that CHIR-99021 promoted mitochondrial adaptation in the obese HLCs by upregulating the expression of the key transcription factors involved in mitochondrial biogenesis.

CHIR-99021 ameliorates hepatic steatosis in obese HLCs

Evidence suggests LD size itself represents a fundamental physical parameter dictating the mechanistic processes used for cellular triacylglycerol catabolism (Gluchowski et al., 2017). The presence of smaller LDs in hepatocyte is intimately linked with a dedicated cytoplasmic repository for the sequestration of toxic-free fatty acids via esterification into triacylglycerol (Rutkowski et al., 2015). Then, the LD size was evaluated in obese HLCs after treatment with CHIR-99021. The results showed that the LD size in the CHIR-

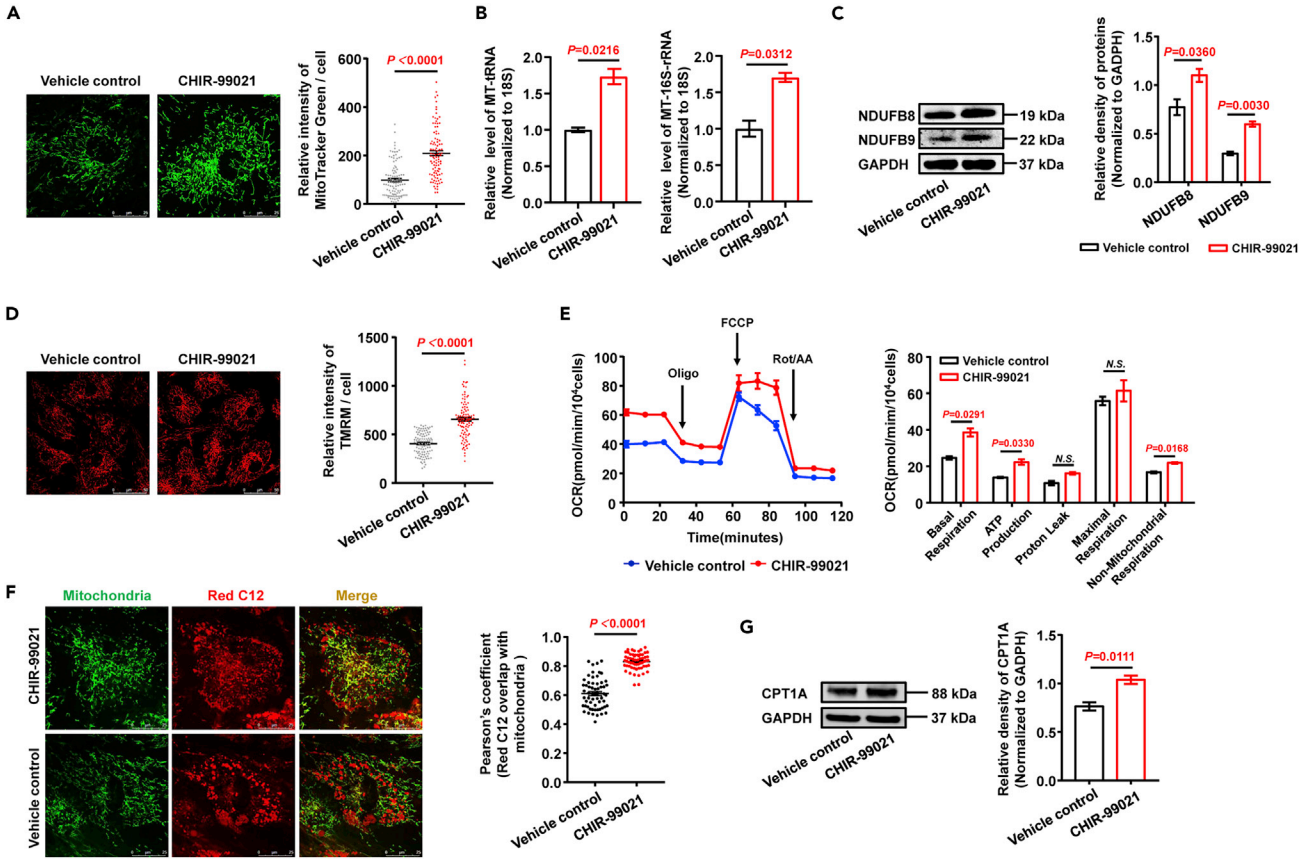

Figure 6. CHIR-99021 promotes mitochondrial biogenesis and function in the obese HLCs

(A) Mitochondrial mass in the CHIR-99021-treated and vehicle-control-treated obese HLCs was determined by MitoTracker Green FM. Scale bars, 25 μm. The fluorescence intensity of MitoTracker Green in each cell was analyzed using ImageJ software. n = 3 different donors; the number of cells was 100 in each group respectively.

(B) Relative mitochondrial DNA content level (measured as mitochondrial tRNA and 16S-rRNA) in the CHIR-99021-treated and vehicle-control-treated obese HLCs was determined by real-time PCR.

(C) Protein levels of NDUFB8 and NDUFB9 in the CHIR-99021-treated and vehicle-control-treated obese HLCs were determined by western blotting. Relative band densities of NDUFB8 and NDUFB9 were normalized to that of GAPDH and analyzed using ImageJ software. n = 3 different donors.

(D) Mitochondrial membrane potential in the CHIR-99021-treated and vehicle-control-treated obese HLCs was determined by TMRM. Scale bars, 50 μm. The fluorescence intensity of TMRM in each cell was analyzed using ImageJ software. n = 3 different donors; the number of cells was 100 in each group respectively.

(E) Kinetic profile of the OCR was measured in the CHIR-99021-treated and vehicle-control-treated obese HLCs using a Seahorse XF Cell Mito Stress test. Black arrows show times of treatment with Oligo, FCCP, Rot, and AA. The basal respiration, ATP production, proton leak, maximal respiration, and non-mitochondrial respiration were calculated. n = 2 different donors.

(F) The CHIR-99021-treated and vehicle-control-treated obese HLCs were incubated with Red C12. Mitochondrial were labeled using MitoTracker Green FM. Fluorescent co-localization of fatty acids and mitochondria represents fatty acid oxidation. Scale bars, 25 μm. The fluorescent co-localization between Red C12 signal and mitochondria in the experiment was quantified by Pearson's coefficient analysis using ImageJ software. n = 3 different donors; the number of cells was 45 in each group respectively.

(G) Protein levels of CPT1A in the CHIR-99021-treated and vehicle-control-treated obese HLCs were determined by western blotting. Relative band densities of CPT1A were normalized to that of GAPDH and analyzed using ImageJ software. n = 3 different donors. Significance compared with the vehicle control, as analyzed by unpaired two-tailed Student's t test. Data are presented as the means ± SEM. Obese HLCs, hepatocyte-like cells derived from adipose stem cell of obese patient; GAPDH, glyceraldehyde-3-phosphate dehydrogenase; NDUFB8, NADH: ubiquinone oxidoreductase subunit B8; NDUFB9, NADH: ubiquinone oxidoreductase subunit B9; OCR, oxygen consumption rate; AA, antimycin A; Oligo, oligomycin; Rot: rotenone; CPT1A, carnitine palmitoyltransferase 1A. See also Figures S12–S17.

99021-treated obese HLCs for 24 h was significant smaller than those in the vehicle-control-treated cells (Figures 8A and S21). Meanwhile, the TG levels were dramatically decreased in the CHIR-99021-treated HLCs for 24 h and 72 h compared with those of the vehicle-control-treated cells (Figures 8B and S22). These findings suggest that CHIR-99021 may ameliorate hepatic steatosis of obese patients.

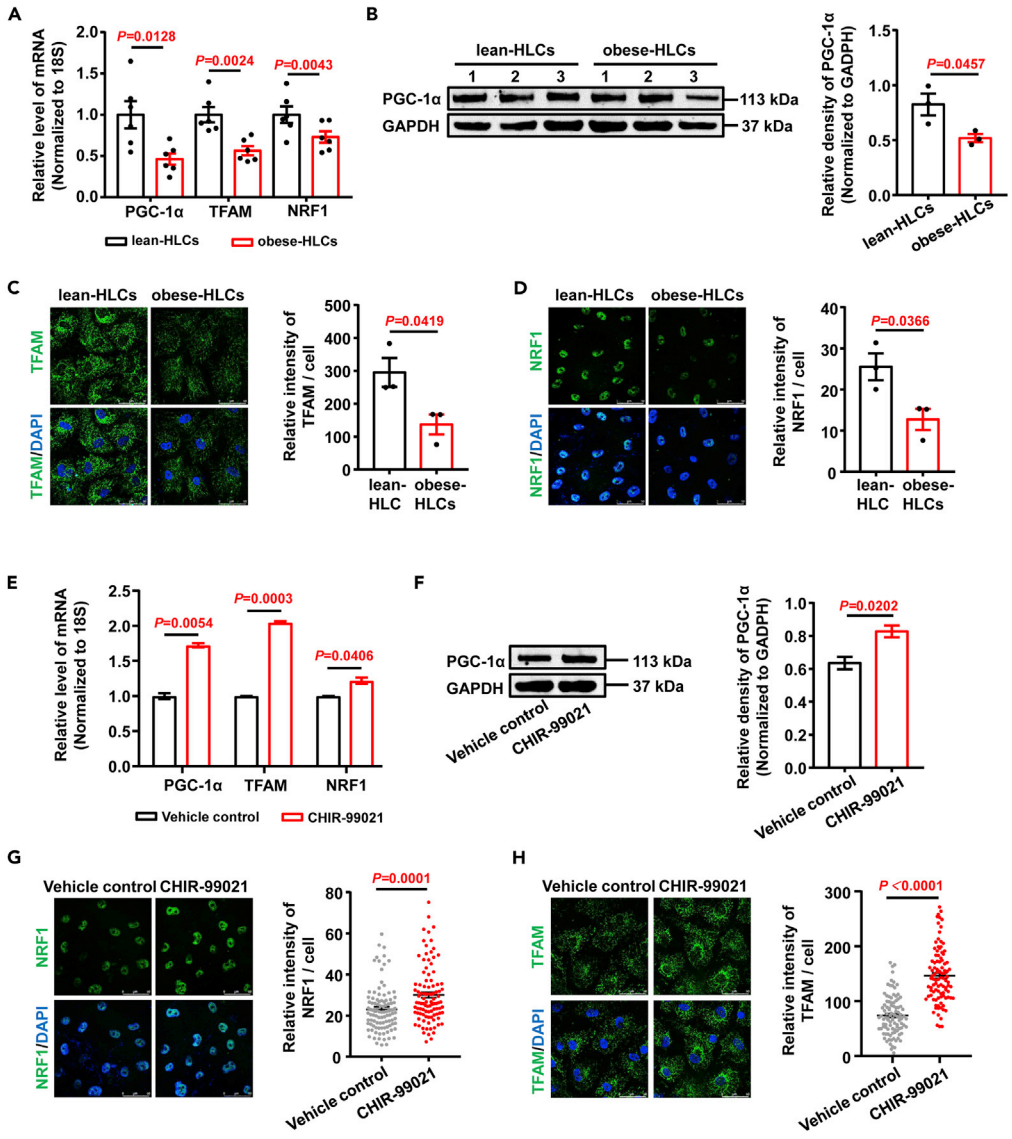

Figure 7. CHIR-99021 upregulates the expression of transcription factors involved in mitochondrial biogenesis in the obese HLCs

(A) Relative mRNA levels of PGC-1α, TFAM, and NRF1 in the lean HLCs and obese HLCs were determined by real-time RT-PCR. n = 6 different donors per group.

(B–D) (B) Protein levels of PGC-1α in the lean HLCs and obese HLCs were determined by western blotting. The relative band density of PGC-1α was normalized to that of GAPDH and analyzed using ImageJ software. n = 3 different donors per group. The relative protein levels of TFAM (C) and NRF1 (D) in the lean HLCs and obese HLCs were determined by immunofluorescence staining. Relative immunofluorescence staining intensity of TFAM and NRF1 in each cell were analyzed using ImageJ software. Scale bars, 50 μm. n = 3 different donors per group; the number of cells was 100 in each donor respectively. See also Figure S18.

(E) Relative mRNA levels of PGC-1α, TFAM, and NRF1 in the CHIR-99021-treated and vehicle-control-treated obese HLCs were determined by real-time RT-PCR.

(F–H) (F) Protein levels of PGC-1α in the CHIR-99021-treated and vehicle-control-treated obese HLCs were determined by western blotting. The relative band density of PGC-1α was normalized to that of GAPDH and was analyzed using ImageJ software. n = 3 different donors. The relative protein levels of NRF1 (G) and TFAM (H) in the CHIR-99021-treated and vehicle-control-treated obese HLCs were determined by immunofluorescence staining. Relative immunofluorescence staining intensity of TFAM and NRF1 in each cell were analyzed using ImageJ software. Scale bars, 50 μm. n = 3 different donors; the number of cells was 100 in each group respectively. Significance compared with the lean HLCs or the vehicle control, as analyzed by unpaired two-tailed Student's t test. Data are presented as the means ± SEM. *N.S.*, not significant.

Figure 7. *Continued*
Lean HLCs, hepatocyte-like cells derived from adipose stem cell of lean donors; obese HLCs, hepatocyte-like cells derived from adipose stem cell of obese patients; PGC-1α, peroxisome-proliferator-activated receptor gamma (PPARγ) coactivator 1 alpha; TFAM, mitochondrial transcription factor A; NRF1, nuclear respiratory factor 1; GAPDH, glyceraldehyde-3-phosphate dehydrogenase.
See also Figures S18–S20.

Taken together, these results suggest that hASCs derived from obese patients can differentiate into HLCs. Obese HLCs exhibit the characteristics of hepatic steatosis. The steatosis of obese HLCs can alter the numerous metabolic pathways regulating hepatic lipids and mitochondrial adaption. CHIR-99021 may ameliorate hepatic steatosis in obese HLCs through the modulation of mitochondrial biogenesis, oxidative function, and fatty acid oxidation by upregulating the expression of the key transcription factors PGC-1α, TFAM, and NRF1 involved in mitochondrial biogenesis and respiratory function. In our opinion, obese HLCs represent an important bridge connecting obesity and FLD and are important to the search for FLD treatments. GSK3 inhibitors may provide a novel treatment strategy for fatty liver disease.

DISCUSSION

Excessive fat deposition in visceral adipose tissue is intimately related to the development of hepatic steatosis in obese individuals and is thought to be a key contributor to the development of FLD and FLD-related cirrhosis and hepatocellular carcinoma (Friedman et al., 2018; Polyzos et al., 2019; Samuel and Shulman, 2018). Therefore, understanding of the processes in obesity that contribute to hepatic steatosis and the search for treatments has increased exponentially (Polyzos et al., 2019; Saltiel and Olefsky, 2017). Given the high variability and complexity of biological, behavioral, and environmental factors among individuals with obesity, studying hepatocytes from individual obese patients is a more valid method for dissecting disease-promoting molecular pathways (Bluher, 2019; Graffmann et al., 2016; Ouchi et al., 2019; Parafati et al., 2018).

Cumulative evidence indicates that HLCs derived from human stem cells may serve as platforms for disease modeling and drug discovery (Corbett and Duncan, 2019; Graffmann et al., 2016; Ouchi et al., 2019; Parafati et al., 2018). Nevertheless, it was not clear whether HLCs from obese individual hASCs have the features of hepatic steatosis. In the present study, we found that HLCs derived from obese patient hASCs exhibit markers typical of hepatocytes and similar to the HLCs from lean donor hASCs. Obese HLCs exhibit the characteristics of hepatic steatosis. More importantly, the upregulated gene expression involved in glycerolipid metabolism, steroid biosynthesis, sphingolipid signaling, cholesterol biosynthetic processes, the positive regulation of interleukin-6 production, and the accumulation of fat droplets identified in the obese HLCs indicated the impairment of intracellular lipid metabolism, which was closely related to the observation in the parenchymal cells of the livers in obese and FLD patients (Iozzo et al., 2010; Latorre et al., 2017). These results suggested that obese HLCs may be influenced by changes in the systemic metabolism status.

Oxidative stress and particularly alterations in mitochondrial function are thought to play significant roles in the simple steatosis to FLD transition (Garcia-Ruiz and Fernandez-Checa, 2018; Mansouri et al., 2018; Sunny et al., 2017). However, the features of maladaptation of mitochondrial oxidative flux are intricate, as documented in patients and experimental models (Koliaki et al., 2015; Rector et al., 2010; Satapati et al., 2015; Yamada et al., 2018). We found that, compared with the lean HLCs, the obese HLCs had altered mitochondrial structure; lower expression of the subunits of mitochondrial complex I, such as NDUFB8 and NDUFB9 (Fiedorczuk and Sazanov, 2018; Piekutowska-Abramczuk et al., 2018); and lower levels of mtDNA; oxidative phosphorylation function (Arruda et al., 2014; Hammerschmidt et al., 2019); mitochondrial ROS (Mansouri et al., 2018), and fatty acid oxidation (Sunny et al., 2017). These indicated that the mitochondrial dysfunction is closely associated with the steatosis in obese HLCs.

The PGC-1 family of regulated coactivators, consisting of PGC-1α, PGC-1β, and PRC, plays a central role in the regulatory network governing the transcriptional control of mitochondrial biogenesis and respiratory functions under cellular stress (Scarpulla, 2011; Wenz, 2013). We found that the mRNA and protein levels of PGC-1α were lower in the obese HLCs than they were in the lean HLCs. Moreover, the expression of NRF1 (also known as NFE2 L1) (Huss and Kelly, 2004), which controls all ten nucleus-encoded cytochrome oxidase subunits, and TFAM (Campbell et al., 2012), a direct regulator of mitochondrial DNA replication and/or transcription, was lower in the obese HLCs than it was in the lean HLCs. These results suggested

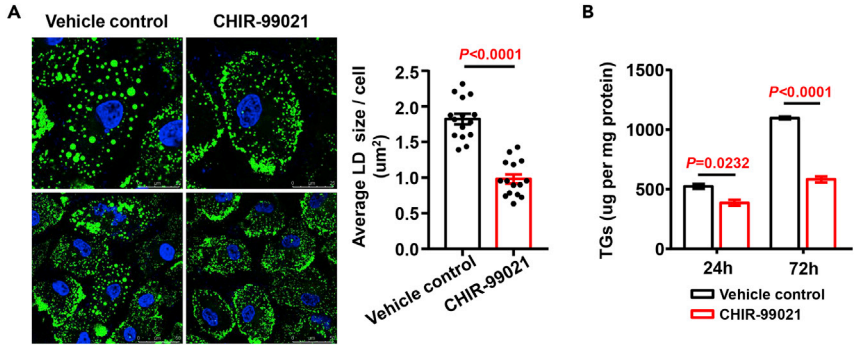

Figure 8. CHIR-99021 ameliorates hepatic steatosis in the obese HLCs

(A) The LDs in the CHIR-99021-treated and vehicle-control-treated obese HLCs were determined by HCS LipidTOX green neutral lipid staining. Scale bars, 50 μm and 25 μm. The average size of LD in each cell was analyzed using ImageJ software. The number of cells was 15 in each group. n = 3 different donors.

(B) TG levels of the CHIR-99021-treated and vehicle-control-treated obese HLCs for 24 h and 72 h were determined by using a triglyceride assay kit. n = 3 different donors. Significance compared with the vehicle control, as analyzed by unpaired two-tailed Student's t test. Data are presented as the means ± SEM. obese HLCs, hepatocyte-like cells derived from adipose stem cell of obese patients; LDs, lipid droplets.

See also Figures S21 and S22.

that mitochondrial dysfunction in the obese HLCs may be influenced by the lower expression of transcription factors PGC-1α, NRF1, and TFAM (Handa et al., 2014; Koliaki et al., 2015).

Previously, we reported that the pharmacological inhibition of GSK-3α and GSK-3β with the specific inhibitor CHIR-99021 promoted mitochondrial biogenesis and oxidative phosphorylation activity during the definitive endodermal differentiation of hASCs (Ma et al., 2019). In this study, we found that CHIR-99021 modified the mitochondrial oxidative phosphorylation activity by upregulating the expression of PGC-1α, NRF1, and TFAM. It has been reported that GSK3β regulates mitochondrial energy metabolism in neurons and glia by altering PGC-1α protein stability, localization, and activity (Martin et al., 2018). Inactivation of GSK-3β enhances skeletal muscle oxidative metabolism (Theeuwes et al., 2017). GSK3β inhibition suppresses hepatic lipid accumulation (Hinds et al., 2016). GSK-3α promotes fatty acid uptake and lipotoxic cardiomyopathy in the context of obesity (Nakamura et al., 2019). These results suggested that mitochondrial dysfunction and steatosis in the obese HLCs may be influenced by the lower expression of these transcription factors, which involved in mitochondrial biogenesis and respiratory function.

Metabolic disorders such as obesity are accompanied by the synthesis and degradation of LDs and can result in the accumulation of significant amounts of lipid deposition, a characteristic feature of hepatocytes in patients with FLD. Maladaptation of mitochondrial oxidative flux is a central feature of hepatic steatosis to FLD transition. Agents targeting mitochondrial dysfunction may provide a novel treatment strategy for hepatic steatosis and NAFLD (Sunny et al., 2017). Herein, we showed that modulating the dysfunction of mitochondrial fatty acid oxidation by CHIR-99021 or GSK3 inhibitors provides an attractive therapeutic strategy for FLD and obesity associated metabolic disease.

Limitations of the study

The mechanism by which CHIR-99021 alleviates steatosis in hepatocytes of obese patients still need to be further explored.

Resource availability

Lead contact

Further information and requests for resources and reagents should be directed to and will be fulfilled by the Lead Contact, Prof. Haiyan Zhang (culture@ccmu.edu.cn).

Materials availability

This study did not generate new unique reagents.

Data and code availability

The datasets generated and/or analyzed during the current study are available in the GEO repository (GSE151760/https://www.ncbi.nlm.nih.gov/geo).

All original, unprocessed images of western blot in the paper were deposited on Mendeley at [https://doi.org/10.17632/54rxxvrwxr.1].

METHODS

All methods can be found in the accompanying Transparent methods supplemental file.

SUPPLEMENTAL INFORMATION

Supplemental information can be found online at https://doi.org/10.1016/j.isci.2021.102149.

ACKNOWLEDGMENTS

This research was supported by The National Natural Science Foundation of China (81770616) and the Beijing Natural Science Foundation (5172009). The authors thank Chenguang Zhang, Ping Wang, Xiao Han, Jun Deng, and Hua Wei for advice in performing these experiments.

AUTHOR CONTRIBUTIONS

YL was responsible for conception and design, collection and assembly of data, and data analysis and writing the manuscript. YL was responsible for collecting the information of patients and data analysis. XH was responsible for perform data analysis of flow cytometry. WL was responsible for administrative support and collection and assembly of data. WY was responsible for collecting the information of patients and data analysis. YM was responsible for performing QPCR assays for mtDNA. XL was responsible for collecting data and histochemistry technical support. XH was responsible for collecting the information of patients and data analysis. RB was responsible for conception and design, data analysis and interpretation, and final approval of the manuscript. HZ was responsible for conception and design, data analysis and interpretation, writing the manuscript, funding acquisition, and final approval of the manuscript. All authors read and approved the final manuscript.

DECLARATION OF INTERESTS

The authors declare that they have no competing interests.

Received: August 8, 2020
Revised: December 30, 2020
Accepted: February 2, 2021
Published: March 19, 2021

REFERENCES

Arruda, A.P., Pers, B.M., Parlakgul, G., Guney, E., Inouye, K., and Hotamisligil, G.S. (2014). Chronic enrichment of hepatic endoplasmic reticulum-mitochondria contact leads to mitochondrial dysfunction in obesity. Nat. Med. *20*, 1427–1435.

Aurich, H., Sgodda, M., Kaltwasser, P., Vetter, M., Weise, A., Liehr, T., Brulport, M., Hengstler, J.G., Dollinger, M.M., Fleig, W.E., et al. (2009). Hepatocyte differentiation of mesenchymal stem cells from human adipose tissue in vitro promotes hepatic integration in vivo. Gut *58*, 570–581.

Banas, A., Teratani, T., Yamamoto, Y., Tokuhara, M., Takeshita, F., Quinn, G., Okochi, H., and Ochiya, T. (2007). Adipose tissue-derived mesenchymal stem cells as a source of human hepatocytes. Hepatology *46*, 219–228.

Bluher, M. (2019). Obesity: global epidemiology and pathogenesis. Nat. Rev. Endocrinol. *15*, 288–298.

Campbell, C.T., Kolesar, J.E., and Kaufman, B.A. (2012). Mitochondrial transcription factor A regulates mitochondrial transcription initiation, DNA packaging, and genome copy number. Biochim. Biophys. Acta *1819*, 921–929.

Corbett, J.L., and Duncan, S.A. (2019). iPSC-derived hepatocytes as a platform for disease modeling and drug discovery. Front. Med. (Lausanne) *6*, 265.

Cusi, K. (2012). Role of obesity and lipotoxicity in the development of nonalcoholic steatohepatitis: pathophysiology and clinical implications. Gastroenterology *142*, 711–725.

Engin, A. (2017). Non-Alcoholic fatty liver disease. Adv. Exp. Med. Biol. *960*, 443–467.

Eslam, M., Valenti, L., and Romeo, S. (2018). Genetics and epigenetics of NAFLD and NASH: clinical impact. J. Hepatol. *68*, 268–279.

Estes, C., Razavi, H., Loomba, R., Younossi, Z., and Sanyal, A.J. (2018). Modeling the epidemic of nonalcoholic fatty liver disease demonstrates an exponential increase in burden of disease. Hepatology *67*, 123–133.

Fan, J.G., Kim, S.U., and Wong, V.W. (2017). New trends on obesity and NAFLD in Asia. J. Hepatol. *67*, 862–873.

Fiedorczuk, K., and Sazanov, L.A. (2018). Mammalian mitochondrial complex I structure and disease-causing mutations. Trends Cell Biol. *28*, 835–867.

Friedman, S.L., Neuschwander-Tetri, B.A., Rinella, M., and Sanyal, A.J. (2018). Mechanisms of NAFLD development and therapeutic strategies. Nat. Med. *24*, 908–922.

Garcia-Ruiz, C., and Fernandez-Checa, J.C. (2018). Mitochondrial oxidative stress and antioxidants balance in fatty liver disease. Hepatol. Commun. *2*, 1425–1439.

Gluchowski, N.L., Becuwe, M., Walther, T.C., and Farese, R.V., Jr. (2017). Lipid droplets and liver disease: from basic biology to clinical implications. Nat. Rev. Gastroenterol. Hepatol. *14*, 343–355.

Graffmann, N., Ring, S., Kawala, M.A., Wruck, W., Ncube, A., Trompeter, H.I., and Adjaye, J. (2016). Modeling nonalcoholic fatty liver disease with human pluripotent stem cell-derived immature hepatocyte-like cells reveals activation of PLIN2 and confirms regulatory functions of peroxisome proliferator-activated receptor alpha. Stem Cells Dev. *25*, 1119–1133.

Grohmann, M., Wiede, F., Dodd, G.T., Gurzov, E.N., Ooi, G.J., Butt, T., Rasmiena, A.A., Kaur, S., Gulati, T., Goh, P.K., et al. (2018). Obesity drives STAT-1-dependent NASH and STAT-3-dependent HCC. Cell *175*, 1289–1306.

Hammerschmidt, P., Ostkotte, D., Nolte, H., Gerl, M.J., Jais, A., Brunner, H.L., Sprenger, H.G., Awazawa, M., Nicholls, H.T., Turpin-Nolan, S.M., et al. (2019). CerS6-Derived sphingolipids interact with mff and promote mitochondrial fragmentation in obesity. Cell *177*, 1536–1552.

Handa, P., Maliken, B.D., Nelson, J.E., Morgan-Stevenson, V., Messner, D.J., Dhillon, B.K., Klintworth, H.M., Beauchamp, M., Yeh, M.M., Elfers, C.T., et al. (2014). Reduced adiponectin signaling due to weight gain results in nonalcoholic steatohepatitis through impaired mitochondrial biogenesis. Hepatology *60*, 133–145.

Hinds, T.D., Jr., Burns, K.A., Hosick, P.A., McBeth, L., Nestor-Kalinoski, A., Drummond, H.A., AlAmodi, A.A., Hankins, M.W., Vanden Heuvel, J.P., and Stec, D.E. (2016). Biliverdin reductase A attenuates hepatic steatosis by inhibition of glycogen synthase kinase (GSK) 3beta phosphorylation of serine 73 of peroxisome proliferator-activated receptor (PPAR) alpha. J. Biol. Chem. *291*, 25179–25191.

Hu, C., Zhao, L., and Li, L. (2019). Current understanding of adipose-derived mesenchymal stem cell-based therapies in liver diseases. Stem Cell Res. Ther. *10*, 199.

Huss, J.M., and Kelly, D.P. (2004). Nuclear receptor signaling and cardiac energetics. Circ. Res. *95*, 568–578.

Iozzo, P., Bucci, M., Roivainen, A., Någren, K., Järvisalo, M.J., Kiss, J., Guiducci, L., Fielding, B., Naum, A.G., Borra, R., et al. (2010). Fatty acid metabolism in the liver, measured by positron emission tomography, is increased in obese individuals. Gastroenterology *139*, 846–856.

Koliaki, C., Szendroedi, J., Kaul, K., Jelenik, T., Nowotny, P., Jankowiak, F., Herder, C., Carstensen, M., Krausch, M., Knoefel, W.T., et al. (2015). Adaptation of hepatic mitochondrial function in humans with non-alcoholic fatty liver is lost in steatohepatitis. Cell Metab. *21*, 739–746.

Latorre, J., Moreno-Navarrete, J.M., Mercader, J.M., Sabater, M., Rovira, O., Girones, J., Ricart, W., Fernandez-Real, J.M., and Ortega, F.J. (2017). Decreased lipid metabolism but increased FA biosynthesis are coupled with changes in liver microRNAs in obese subjects with NAFLD. Int. J. Obes. (Lond) *41*, 620–630.

Li, H., Zhu, L., Chen, H., Li, T., Han, Q., Wang, S., Yao, X., Feng, H., Fan, L., Gao, S., et al. (2018). Generation of functional hepatocytes from human adipose-derived MYC (+) KLF4(+) GMNN (+) stem cells analyzed by single-cell RNA-seq profiling. Stem Cells Transl. Med. *7*, 792–805.

Li, X., Yuan, J., Li, W., Liu, S., Hua, M., Lu, X., and Zhang, H. (2014). Direct differentiation of homogeneous human adipose stem cells into functional hepatocytes by mimicking liver embryogenesis. J. Cell Physiol. *229*, 801–812.

Louwen, F., Ritter, A., Kreis, N.N., and Yuan, J. (2018). Insight into the development of obesity: functional alterations of adipose-derived mesenchymal stem cells. Obes. Rev. *19*, 888–904.

Ma, Y., Ma, M., Sun, J., Li, W., Li, Y., Guo, X., and Zhang, H. (2019). CHIR-99021 regulates mitochondrial remodelling via beta-catenin signalling and miRNA expression during endodermal differentiation. J. Cell Sci. *132*, jcs229948.

Mansouri, A., Gattolliat, C.H., and Asselah, T. (2018). Mitochondrial dysfunction and signaling in chronic liver diseases. Gastroenterology *155*, 629–647.

Martin, S.A., Souder, D.C., Miller, K.N., Clark, J.P., Sagar, A.K., Eliceiri, K.W., Puglielli, L., Beasley, T.M., and Anderson, R.M. (2018). GSK3beta regulates brain energy metabolism. Cell Rep. *23*, 1922–1931.

Nakamura, M., Liu, T., Husain, S., Zhai, P., Warren, J.S., Hsu, C.P., Matsuda, T., Phiel, C.J., Cox, J.E., Tian, B., et al. (2019). Glycogen synthase kinase-3alpha promotes fatty acid uptake and lipotoxic cardiomyopathy. Cell Metab. *29*, 1119–1134.

Oñate, B., Vilahur, G., Camino-López, S., Díez-Caballero, A., Ballesta-López, C., Ybarra, J., Moscatiello, F., Herrero, J., and Badimon, L. (2013). Stem cells isolated from adipose tissue of obese patients show changes in their transcriptomic profile that indicate loss in stemcellness and increased commitment to an adipocyte-like phenotype. BMC Genomics *14*, 1–12.

Ouchi, R., Togo, S., Kimura, M., Shinozawa, T., Koido, M., Koike, H., Thompson, W., Karns, R.A., Mayhew, C.N., McGrath, P.S., et al. (2019). Modeling steatohepatitis in humans with pluripotent stem cell-derived Organoids. Cell Metab. *30*, 374–384.

Pachon-Pena, G., Serena, C., Ejarque, M., Petriz, J., Duran, X., Oliva-Olivera, W., Simo, R., Tinahones, F.J., Fernandez-Veledo, S., and Vendrell, J. (2016). Obesity determines the immunophenotypic profile and functional characteristics of human mesenchymal stem cells from adipose tissue. Stem Cells Transl. Med. *5*, 464–475.

Parafati, M., Kirby, R.J., Khorasanizadeh, S., Rastinejad, F., and Malany, S. (2018). A nonalcoholic fatty liver disease model in human induced pluripotent stem cell-derived hepatocytes, created by endoplasmic reticulum stress-induced steatosis. Dis. Model. Mech. *11*, dmm033530.

Piekutowska-Abramczuk, D., Assouline, Z., Matakovic, L., Feichtinger, R.G., Konarikova, E., Jurkiewicz, E., Stawinski, P., Gusic, M., Koller, A., Pollak, A., et al. (2018). NDUFB8 mutations cause mitochondrial complex I deficiency in individuals with leigh-like encephalomyopathy. Am. J. Hum. Genet. *102*, 460–467.

Polyzos, S.A., Kountouras, J., and Mantzoros, C.S. (2019). Obesity and nonalcoholic fattyliver disease: from pathophysiology to therapeutics. Metabolism *92*, 82–97.

Rambold, A.S., Cohen, S., and Lippincott-Schwartz, J. (2015). Fatty acid trafficking in starved cells: regulation by lipid droplet lipolysis, autophagy, and mitochondrial fusion dynamics. Dev. Cell. *32*, 678–692.

Rector, R.S., Thyfault, J.P., Uptergrove, G.M., Morris, E.M., Naples, S.P., Borengasser, S.J., Mikus, C.R., Laye, M.J., Laughlin, M.H., Booth, F.W., et al. (2010). Mitochondrial dysfunction precedes insulin resistance and hepatic steatosis and contributes to the natural history of non-alcoholic fatty liver disease in an obese rodent model. J. Hepatol. *52*, 727–736.

Ritter, A., Friemel, A., Kreis, N.N., Hoock, S.C., Roth, S., Kielland-Kaisen, U., Bruggmann, D., Solbach, C., Louwen, F., and Yuan, J. (2018). Primary cilia are dysfunctional in obese adipose-derived mesenchymal stem cells. Stem Cell Rep. *10*, 583–599.

Rutkowski, J.M., Stern, J.H., and Scherer, P.E. (2015). The cell biology of fat expansion. J. Cell Biol. *208*, 501–512.

Saltiel, A.R., and Olefsky, J.M. (2017). Inflammatory mechanisms linking obesity and metabolic disease. J. Clin. Invest. *127*, 1–4.

Samuel, V.T., and Shulman, G.I. (2018). Nonalcoholic fatty liver disease as a nexus of metabolic and hepatic diseases. Cell Metab. *27*, 22–41.

Satapati, S., Kucejova, B., Duarte, J.A., Fletcher, J.A., Reynolds, L., Sunny, N.E., He, T., Nair, L.A., Livingston, K.A., Fu, X., et al. (2015). Mitochondrial metabolism mediates oxidative stress and inflammation in fatty liver. J. Clin. Invest. *125*, 4447–4462.

Scarpulla, R.C. (2011). Metabolic control of mitochondrial biogenesis through the PGC-1 family regulatory network. Biochim. Biophys. Acta *1813*, 1269–1278.

Seo, M.J., Suh, S.Y., Bae, Y.C., and Jung, J.S. (2005). Differentiation of human adipose stromal cells into hepatic lineage in vitro and in vivo. Biochem. Biophys. Res. Commun. *328*, 258–264.

Serena, C., Keiran, N., Ceperuelo-Mallafre, V., Ejarque, M., Fradera, R., Roche, K., Nunez-Roa, C., Vendrell, J., and Fernandez-Veledo, S. (2016). Obesity and type 2 diabetes alters the immune properties of human adipose derived stem cells. Stem Cells *34*, 2559–2573.

Serena, C., Keiran, N., Madeira, A., Maymo-Masip, E., Ejarque, M., Terron-Puig, M., Espin, E., Marti, M., Borruel, N., Guarner, F., et al. (2017). Crohn's disease disturbs the immune properties of human adipose-

derived stem cells related to inflammasome activation. Stem Cell Rep. *9*, 1109–1123.

Singh, S., Allen, A.M., Wang, Z., Prokop, L.J., Murad, M.H., and Loomba, R. (2015). Fibrosis progression in nonalcoholic fatty liver vs nonalcoholic steatohepatitis: a systematic review and meta-analysis of paired-biopsy studies. Clin. Gastroenterol. Hepatol. *13*, 643–654.

Sunny, N.E., Bril, F., and Cusi, K. (2017). Mitochondrial adaptation in nonalcoholic fatty liver disease: novel mechanisms and treatment strategies. Trends Endocrinol. Metab. *28*, 250–260.

Theeuwes, W.F., Gosker, H.R., Langen, R.C.J., Verhees, K.J.P., Pansters, N.A.M., Schols, A., and Remels, A.H.V. (2017). Inactivation of glycogen synthase kinase-3beta (GSK-3beta) enhances skeletal muscle oxidative metabolism. Biochim. Biophys. Acta Mol. Basis Dis. *1863*, 3075–3086.

Wenz, T. (2013). Regulation of mitochondrial biogenesis and PGC-1alpha under cellular stress. Mitochondrion *13*, 134–142.

Yamada, T., Murata, D., Adachi, Y., Itoh, K., Kameoka, S., Igarashi, A., Kato, T., Araki, Y., Huganir, R.L., Dawson, T.M., et al. (2018). Mitochondrial stasis reveals p62-mediated Ubiquitination in parkin-independent mitophagy and mitigates nonalcoholic fatty liver disease. Cell Metab. *28*, 588–604.

Yuan, J., Li, W., Huang, J., Guo, X., Li, X., Lu, X., Huang, X., and Zhang, H. (2015). Transplantation of human adipose stem cell-derived hepatocyte-like cells with restricted localization to liver using acellular amniotic membrane. Stem Cell Res. Ther. *6*, 217.

iScience, Volume *24*

Supplemental Information

GSK3 inhibitor ameliorates steatosis through the modulation of mitochondrial dysfunction in hepatocytes of obese patients

Yaqiong Li, Yi Lin, Xueya Han, Weihong Li, Wenmao Yan, Yuejiao Ma, Xin Lu, Xiaowu Huang, Rixing Bai, and Haiyan Zhang

Supplemental Figures and Figure Legends

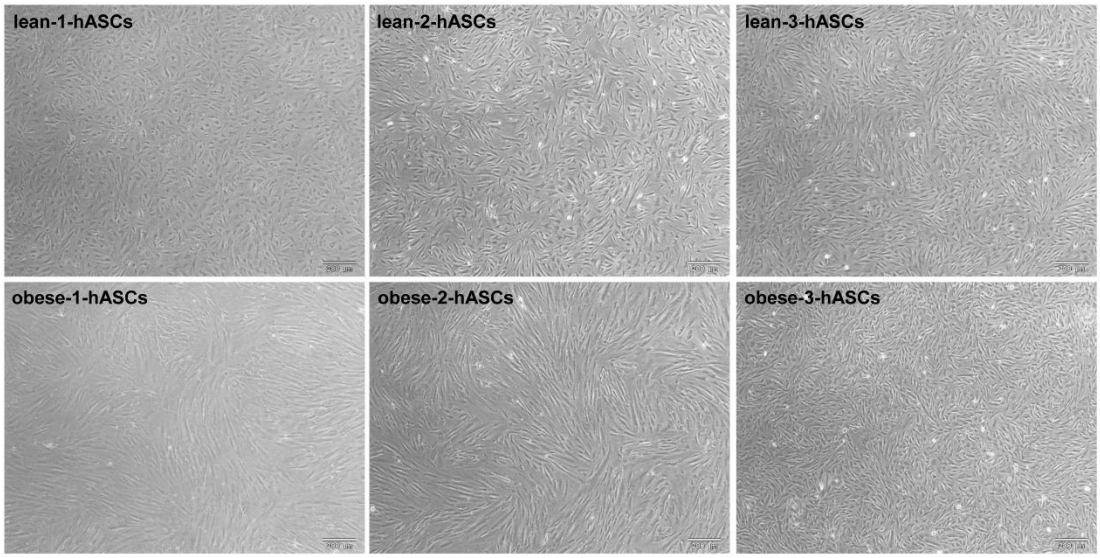

Figure S1. The morphological properties of hASCs from lean donors and obese donors were determined using phase-contrast microscopy, Related to Figure 1. Scale bars, 200 um. n=3 different donors per group. hASCs, human adipose stem cells.

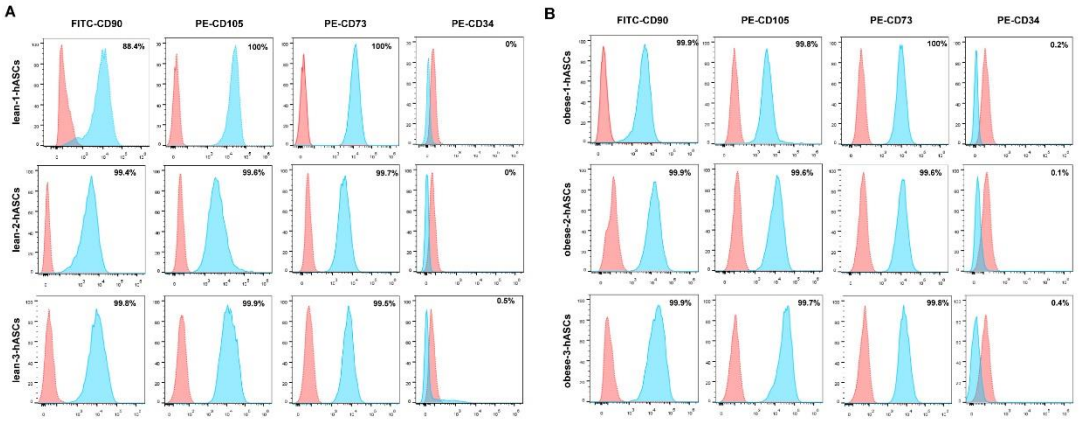

Figure S2. Immunophenotype of hASCs from lean donors and obese donors were determined using flow cytometry, Related to Figure 1. hASCs from lean donors (A), obese donors (B) at passage 6 were labeled with antibodies against the indicated antigens and analyzed using flow cytometry. The percentage of cells staining positive is indicated in the upper right corner of each part. The cyan line indicates positive-staining cells, whereas the red line indicates the isotype-matched monoclonal antibody control. n=3 different donors per group. hASCs, human adipose stem cells; FITC, fluorescein isothiocyanate; PE, phycoerythrin.

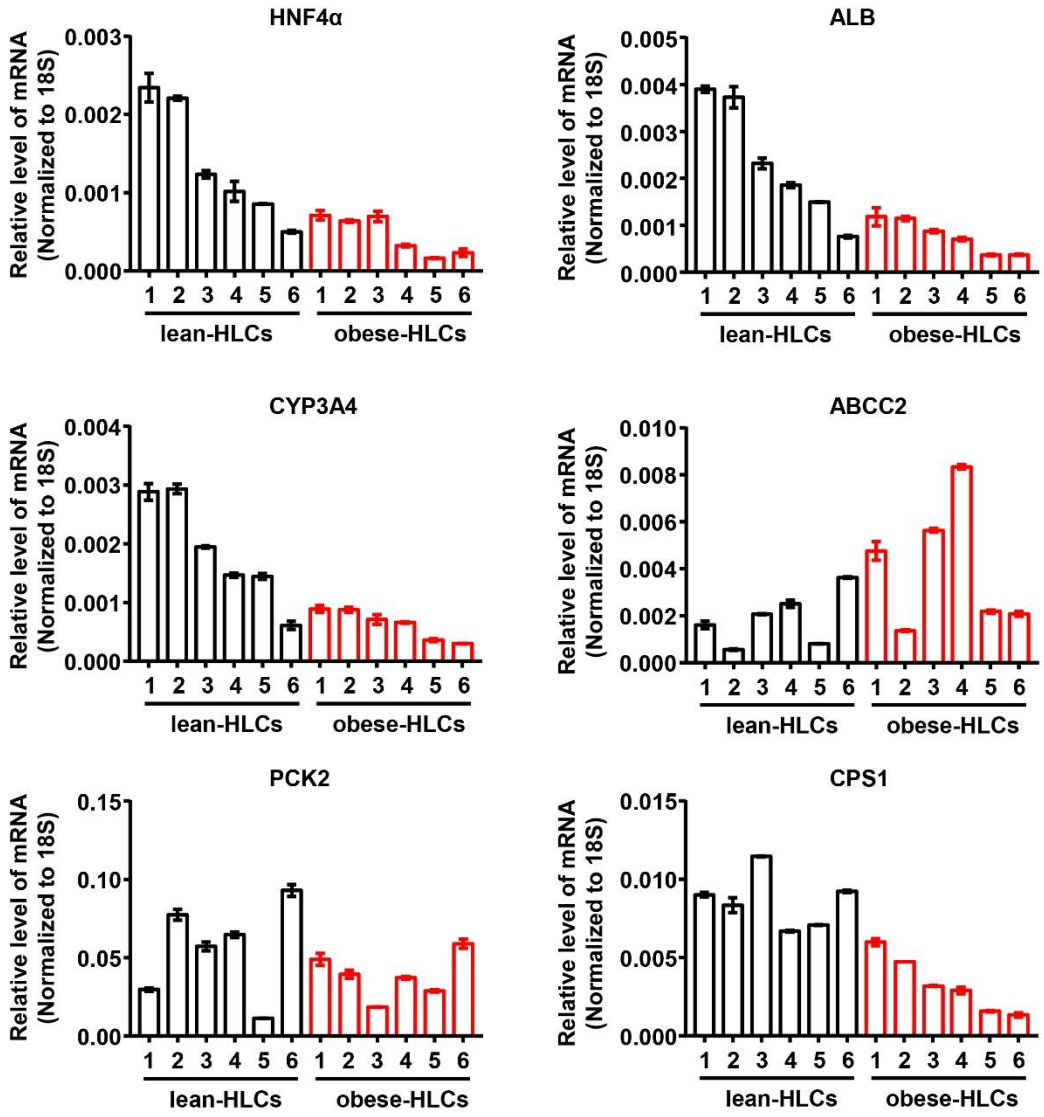

Figure S3. The mRNA levels of hepatic markers in the lean HLCs and obese HLCs were determined by real-time RT-PCR, Related to Figure 1. The relative expression of each gene was normalized against 18S rRNA. Data are presented as the means ± SEM. n=6 different donors per group. lean HLCs, hepatocyte-like cells derived from adipose stem cell of lean donors; obese HLCs, hepatocyte-like cells derived from adipose stem cell of obese patients; HNF4α, hepatocyte nuclear factor 4 alpha; ALB, albumin; CYP3A4, cytochrome P450 family 3 subfamily A member 4; ABCC2, ATP-binding cassette, sub-family C (CFTR/MRP), member 2; PCK2, phosphoenolpyruvate carboxykinase 2; CPS1, carbamoyl-phosphate synthase1.

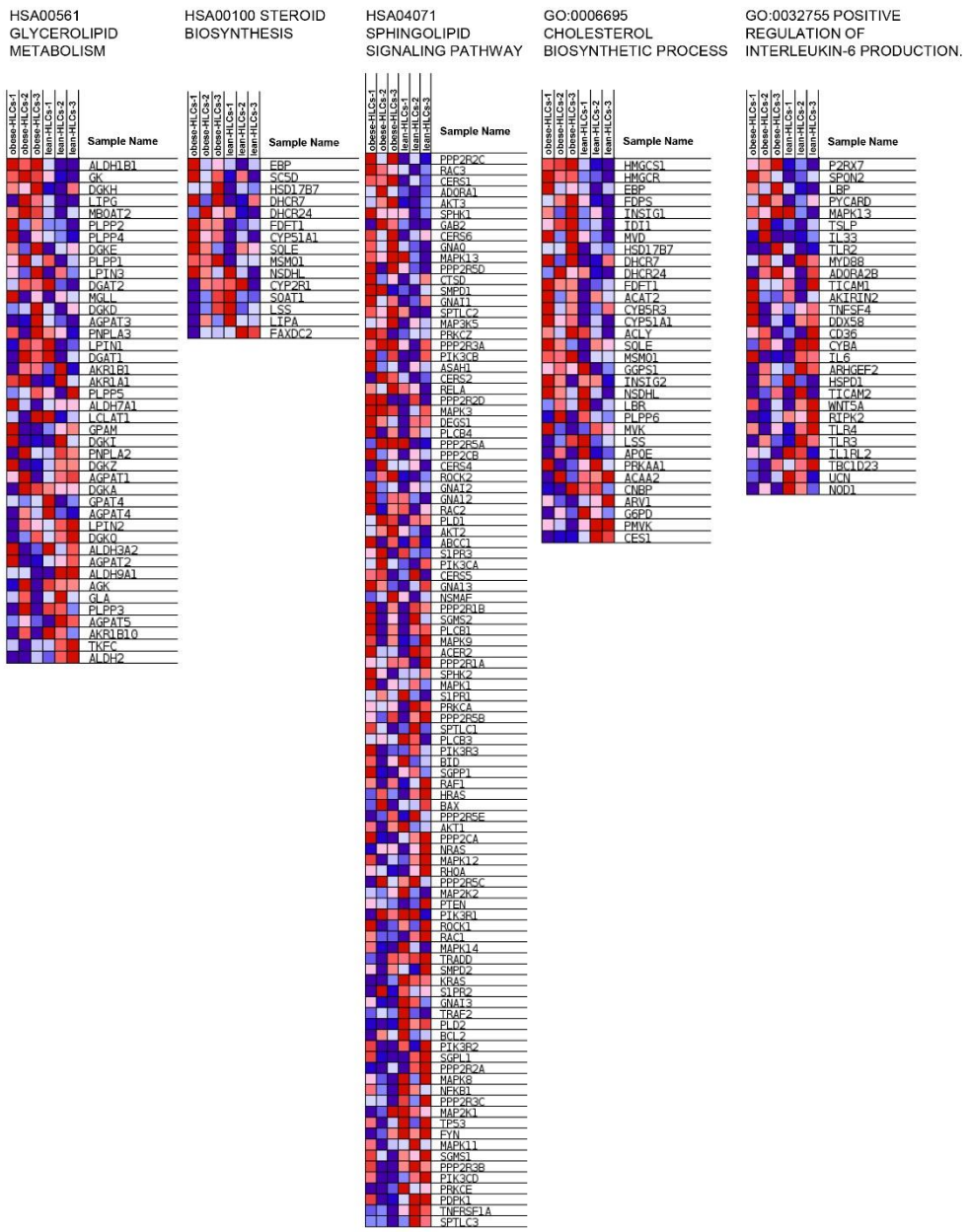

Figure S4. Heatmap generated by the common genes shared between two groups based on the upregulated pathways or biology processes (Figure 2D) in the obese HLCs, Related to Figure 2. In the heatmap, high expression is depicted in red and low expression is depicted in blue. The columns are log10 plot of the normalized intensity of triplicate samples for each group. n=3 different donors per group. lean HLCs, hepatocyte-like cells derived from adipose stem cell of lean patients; obese HLCs, hepatocyte-like cells derived from adipose stem cell of obese patients.

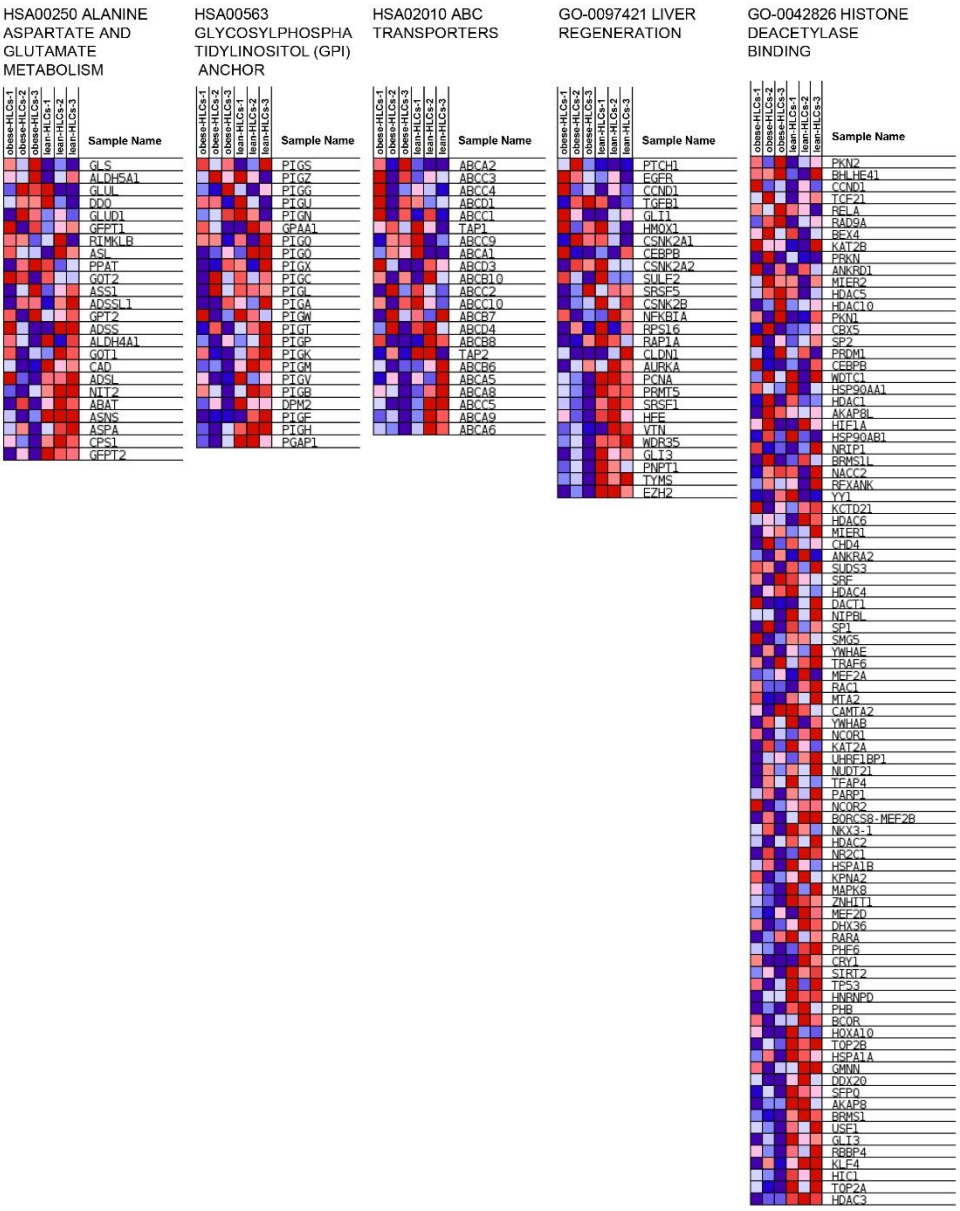

Figure S5 Heatmap generated by the common genes shared between two groups based on the downregulated pathways or biology processes (Figure 2E) in the obese HLCs, Related to Figure 2. In the heatmap, high expression is depicted in red and low expression is depicted in blue. The columns are log10 plot of the normalized intensity of triplicate samples for each group. n=3 different donors per group. lean HLCs, hepatocyte-like cells derived from adipose stem cell of lean patients; obese HLCs, hepatocyte-like cells derived from adipose stem cell of obese patients.

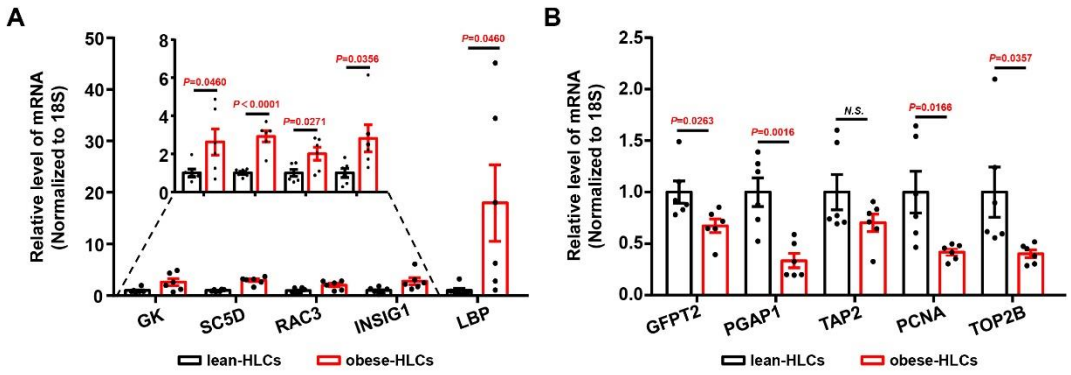

Figure S6. The mRNA levels of ten interest differentiated expressed genes were confirmed by real-time RT-PCR, Related to Figure 2. (A) Relative mRNA levels of GK, SC5D, RAC3, INSIG1 and LBP in the lean HLCs and obese HLCs were determined by real-time RT-PCR. n=6 different donors per group. (B) Relative mRNA levels of GFPT2, PGAP1, TAP2, PCNA and TOP2B in the lean HLCs and obese HLCs were determined by real-time RT-PCR. n=6 different donors per group. The relative expression of each gene was normalized against 18S rRNA. Data are presented as the means ± SEM. Statistical significance compared to the lean HLCs, as analysed by unpaired two-tailed Student's t-test. GK, glycerol kinase; SC5D, sterol-C5-desaturase; RAC3, Rac family small GTPase 3; INSIG1, insulin induced gene 1; LBP, lipopolysaccharide binding protein; GFPT2, glutamine-fructose-6-phosphate transaminase 2; PGAP1, post-GPI attachment to proteins inositol deacylase 1; TAP2, transporter 2, ATP binding cassette subfamily B member; PCNA, proliferating cell nuclear antigen; TOP2B, DNA topoisomerase II beta. lean HLCs, hepatocyte-like cells derived from adipose stem cell of lean donors; obese HLCs, hepatocyte-like cells derived from adipose stem cell of obese patients;

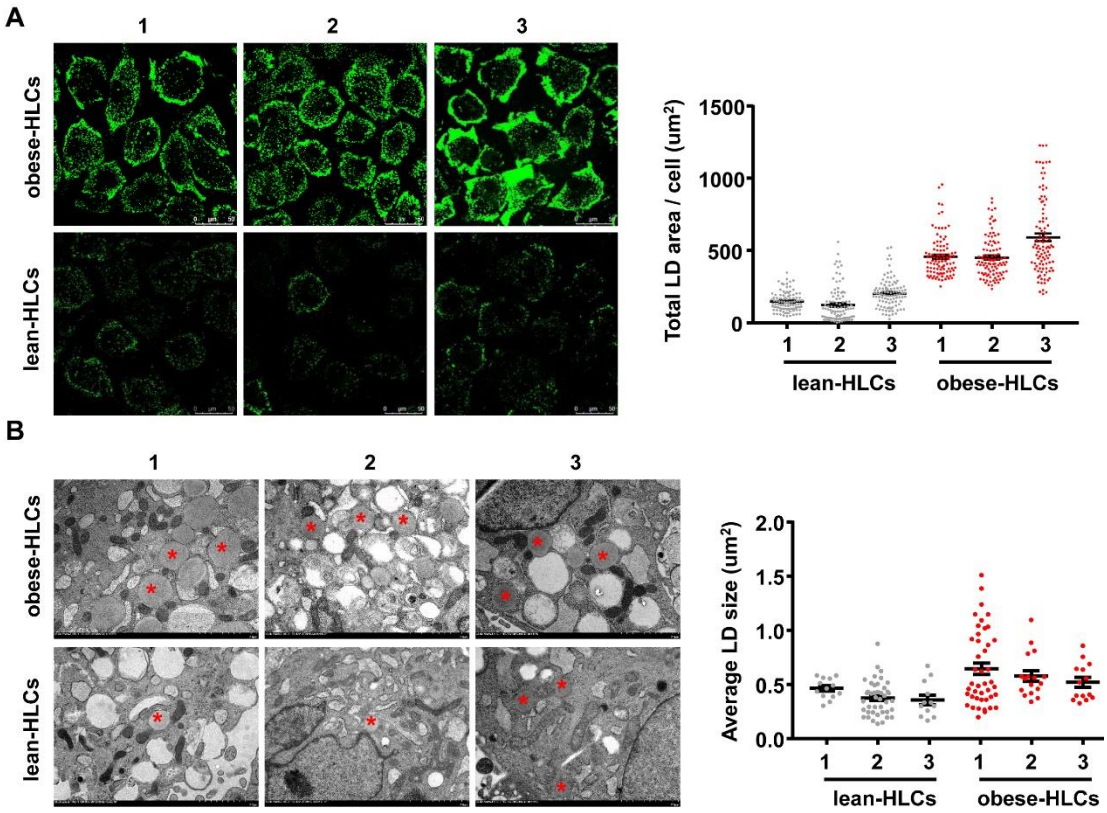

Figure S7. LDs in HLCs derived from lean donors and obese donors were determined, Related to Figure 3. (A) LDs in HLCs from lean donors and obese donors were determined by HCS LipidTOX™ green neutral lipid staining. Total LD area in each cell was analysed using ImageJ software. Scale bars, 50 um. Data are presented as the means ± SEM. n=3 different donors per group, the number of cells was 100 in each donor respectively. (B) The size of LD in HLCs from three lean donors and three obese donors was determined using TEM. The red asterisk indicates an LD. The average LD size in the cells was determined using ImageJ software. Scale bars, 2 um. n=3 different donors per group, the number of LDs was 13, 42, 12 in the lean group and was 43, 17, 14 in the obese group respectively. Data are presented as the means ± SEM. lean HLCs, hepatocyte-like cells derived from adipose stem cell of lean donors; obese HLCs, hepatocyte-like cells derived from adipose stem cell of obese patients; LDs, lipid droplets; TEM, transmission electron microscopy.

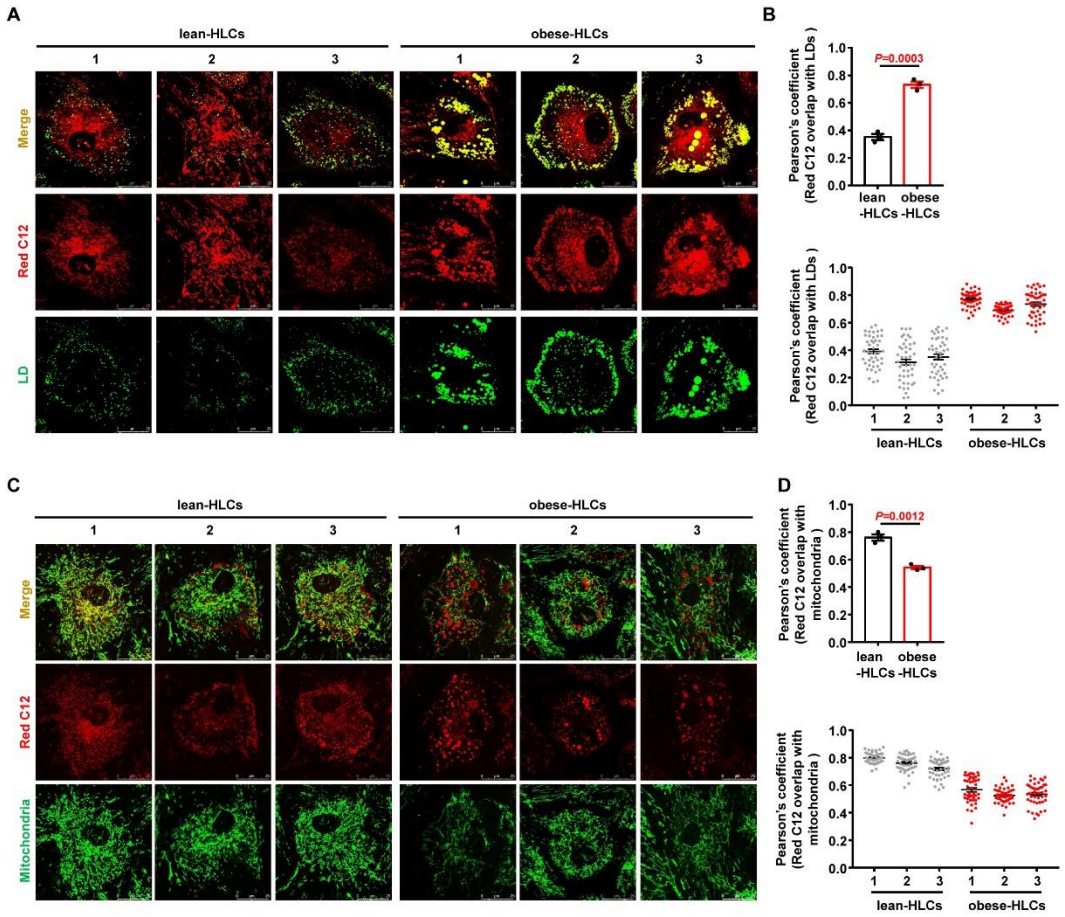

Figure S8. Lipogenesis and fatty acid oxidation in the HLCs were determined, Related to Figure 3. (A) FAs were labeled using BODIPY 558/568 C_{12} (Red C12) and LDs were labeled using HCS LipidTOX™ green neutral lipid stain. Scale bars, 25 μm. (B) The fluorescent co-localization between Red C12 signal and LDs in the experiment was quantified by Pearson's coefficient analysis using ImageJ software. n=3 different donors per group, the number of cells was 45 in each donor respectively. (C) Mitochondrial were labeled using MitoTracker Green FM. Scale bars, 25 μm. (D) The fluorescent co-localization between Red C12 signal and mitochondria in the experiment was quantified by Pearson's coefficient analysis using ImageJ software. n=3 different donors per group, the number of cells was 45 in each donor respectively. Significance compared to the lean HLCs. Data are presented as the means ± SEM. lean HLCs, hepatocyte-like cells derived from adipose stem cell of lean donors; obese HLCs, hepatocyte-like cells derived from adipose stem cell of obese patients.

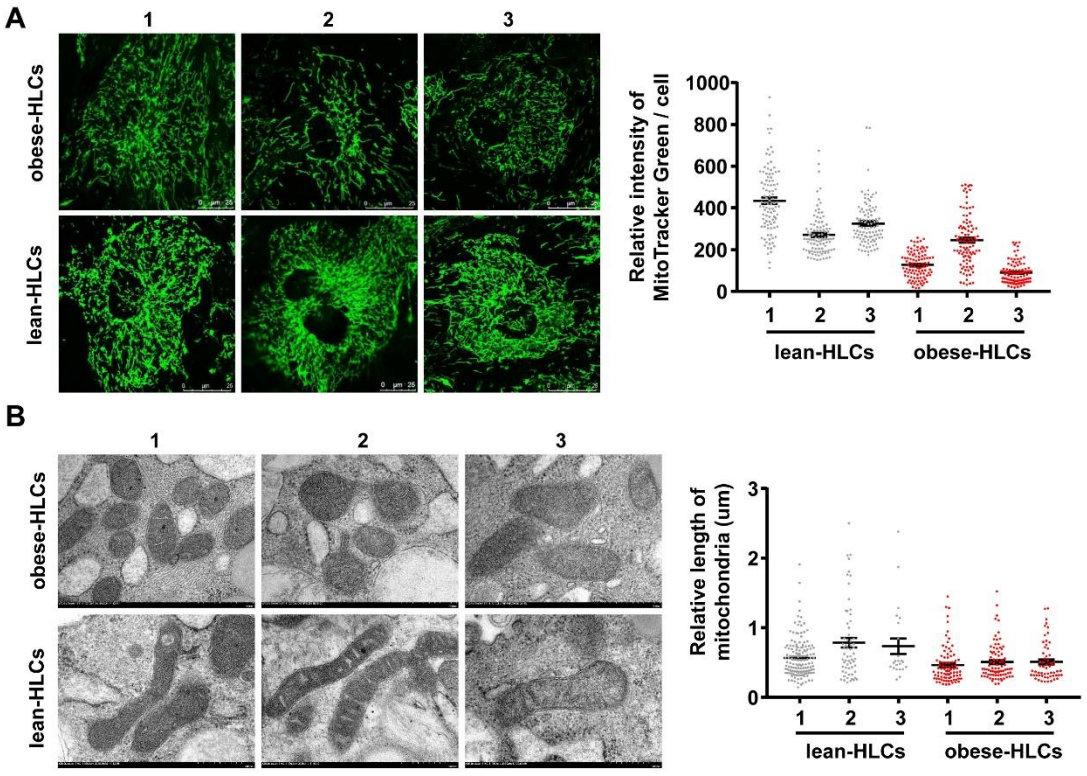

Figure S9. Mitochondrial mass and morphology in the HLCs were determined, Related to Figure 4. (A) Mitochondrial mass in the HLCs from three lean donors and three obese donors was determined by MitoTracker Green FM. Scale bars, 25 μm. The fluorescence intensity of MitoTracker Green in each cell was analysed using ImageJ software. n=3 different donors per group, the number of cells was 100 in each donor respectively. (B) Mitochondrial morphology in the HLCs from three lean donors and three obese donors was determined using TEM. The relative length of mitochondria in the cells was determined using ImageJ software. Scale bars, 500 nm. n=3 different donors per group, the number of mitochondria was 145, 62, 23 in the lean group and was 85, 86, 59 in the obese group respectively. Data are presented as the means ± SEM. lean HLCs, hepatocyte-like cells derived from adipose stem cell of lean donors; obese HLCs, hepatocyte-like cells derived from adipose stem cell of obese patients.

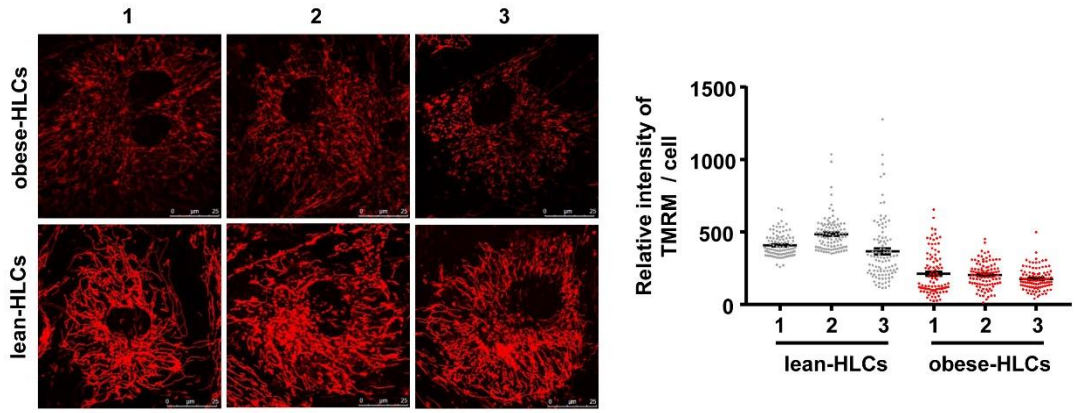

Figure S10. Mitochondrial potential in the HLCs was determined, Related to Figure 4. Scale bars, 25 μm. The fluorescence intensity of TMRM in each cell was analysed using ImageJ software. n=3 different donors per group, the number of cells was 100 in each donor respectively. Data are presented as the means ± SEM. lean HLCs, hepatocyte-like cells derived from adipose stem cell of lean donors; obese HLCs, hepatocyte-like cells derived from adipose stem cell of obese patients; TMRM, Tetramethylrhodamine, methyl ester.

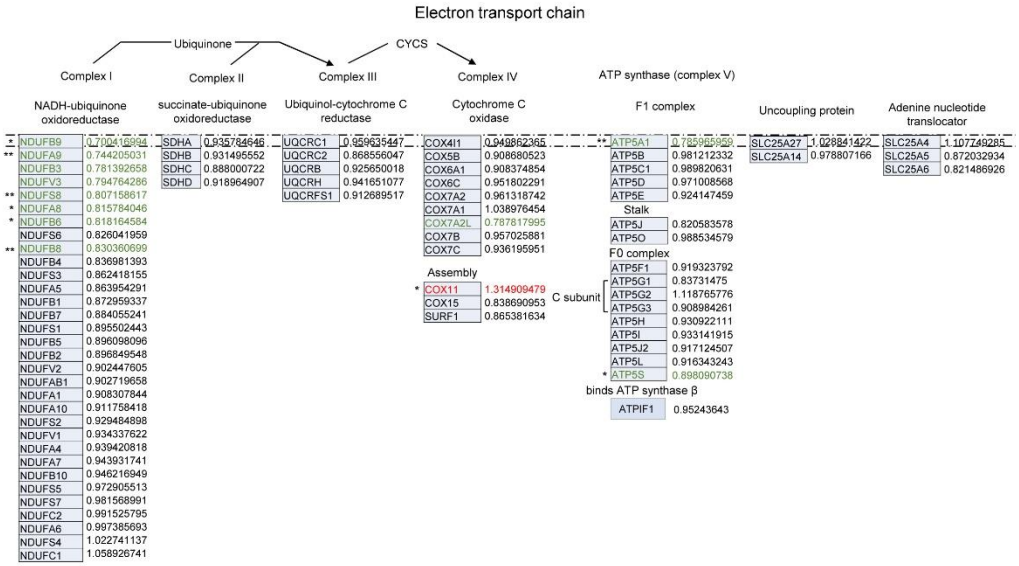

Figure S11. The relative mRNA level of genes involved in oxidative phosphorylation in the obese HLCs, Related to Figure 5. The fold changes presented beside the names of the genes. Upregulated genes are shown in red, and downregulated genes are shown in green. n=3 different donors per group. Statistical significance compared to the lean-HLCs. **P<0.05, **P<0.01.* obese HLCs, hepatocyte-like cells derived from adipose stem cell of obese patients; COX, cytochrome c oxidase; CYCS, cytochrome c, somatic; NDUF, NADH: ubiquinone oxidoreductase; SDH, succinate dehydrogenase complex; SLC, solute carrier; SURF, cytochrome c oxidase assembly factor; UQCR, ubiquinol-cytochrome c reductase.

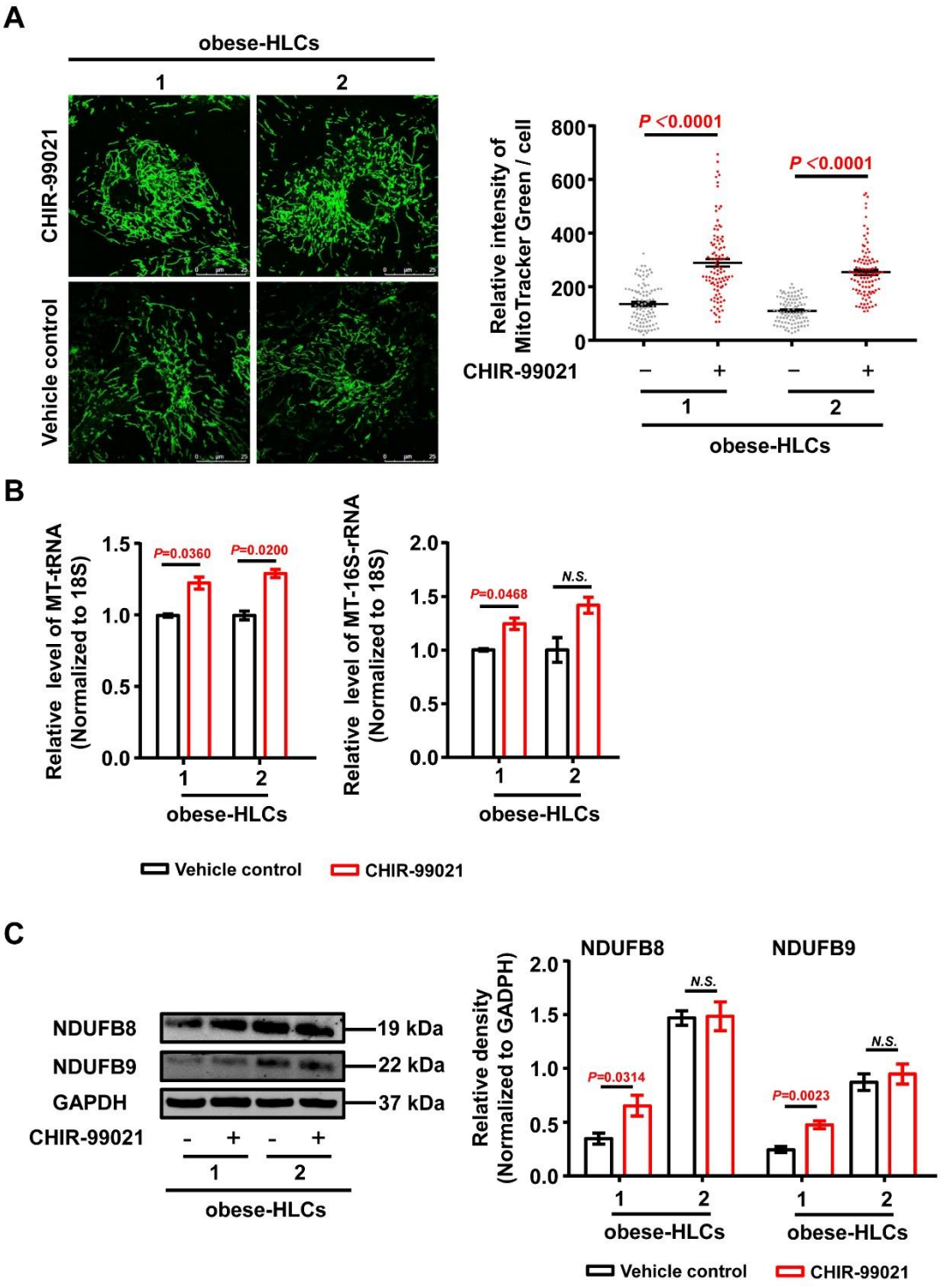

Figure S12. The mitochondrial contents were determined in obese HLCs, Related to Figure 6. (A) Mitochondrial mass in the CHIR-99021-treated and vehicle control-treated obese HLCs was determined using MitoTracker Green FM. Scale bars, 25 μm. The fluorescence intensity of MitoTracker Green in each cell was analysed using ImageJ software. n=2 different donors, the number of cells was 100 in each group respectively. (B) Relative mitochondrial DNA content levels (measured as mitochondrial tRNA and 16S-rRNA) in the CHIR-99021-treated and vehicle control-treated obese HLCs were determined by real-time PCR. n=2 different donors. (C) Protein levels of NDUFB8 and NDUFB9 in the CHIR-99021-

treated and vehicle control-treated obese HLCs were determined by western blotting. Relative band densities of NDUFB8 and NDUFB9 were normalized to that of GAPDH and were analysed using ImageJ software. n=2 different donors. Significance compared to the vehicle control. *N.S.*, not significant. Data are presented as the means ± SEM. obese HLCs, hepatocyte-like cells derived from adipose stem cell of obese patients; GAPDH, glyceraldehyde-3-phosphate dehydrogenase; NDUFB8, NADH: ubiquinone oxidoreductase subunit B8; NDUFB9, NADH: ubiquinone oxidoreductase subunit B9.

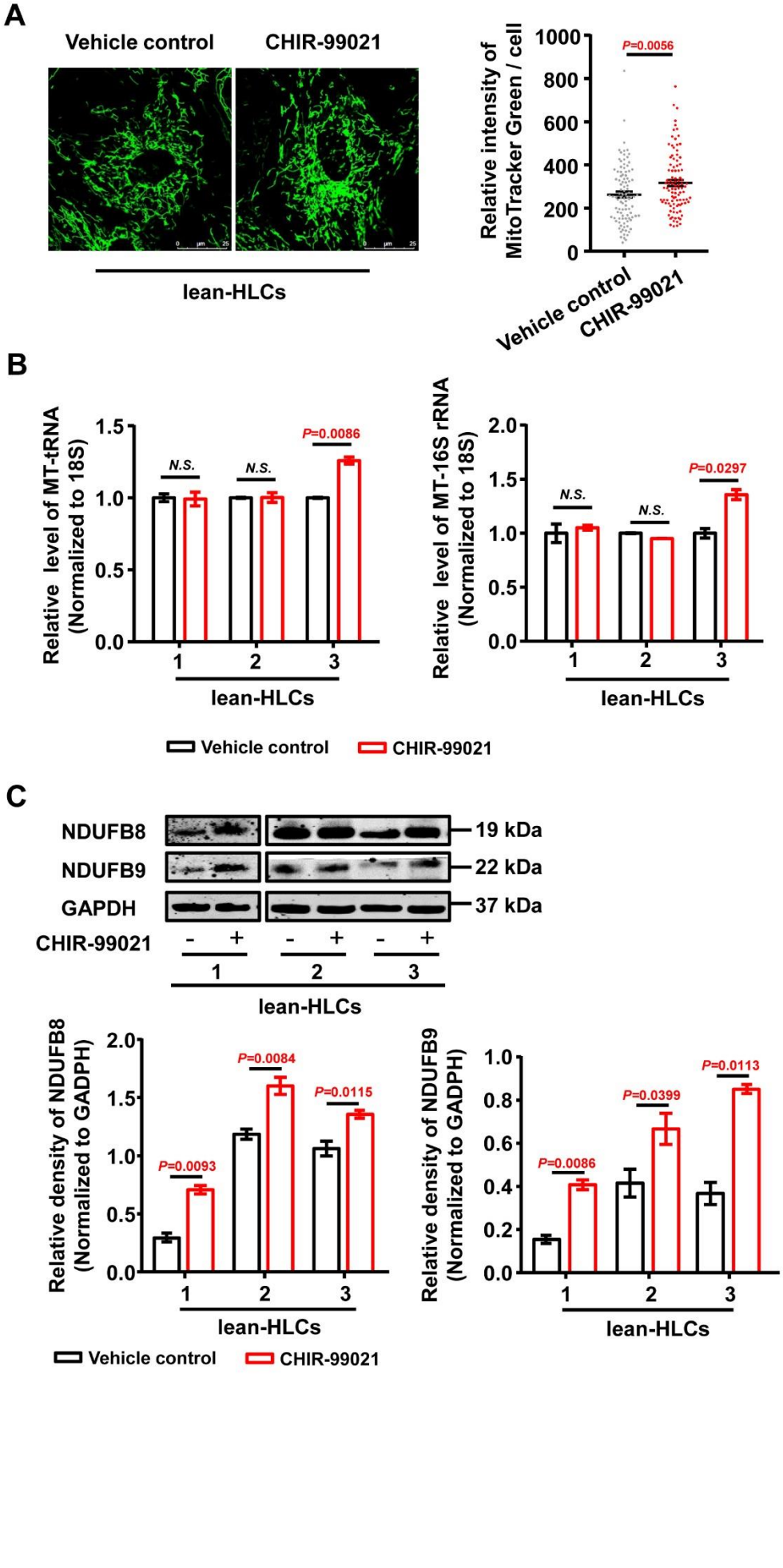
A
Vehicle control
CHIR-99021
lean-HLCs
Relative intensity of MitoTracker Green / cell
P=0.0056
Vehicle control
CHIR-99021
B
Relative level of MT-tRNA (Normalized to 18S)
N.S.
N.S.
P=0.0086
lean-HLCs
Relative level of MT-16S rRNA (Normalized to 18S)
N.S.
N.S.
P=0.0297
lean-HLCs
Vehicle control
CHIR-99021
C
NDUFB8
NDUFB9
GAPDH
19 kDa
22 kDa
37 kDa
CHIR-99021
lean-HLCs
Relative density of NDUFB8 (Normalized to GADPH)
P=0.0093
P=0.0084
P=0.0115
lean-HLCs
Relative density of NDUFB9 (Normalized to GADPH)
P=0.0086
P=0.0399
P=0.0113
lean-HLCs
Vehicle control
CHIR-99021

Figure S13. The mitochondrial contents were determined in lean HLCs, Related to Figure 6. (A) Mitochondrial mass in the CHIR-99021-treated and vehicle control-treated lean HLCs was determined by MitoTracker Green FM. Scale bars, 25 μm. The fluorescence intensity of MitoTracker Green in each cell was analysed using ImageJ software. The number of cells was 100 in each group respectively. (B) Relative mitochondrial DNA content level (measured as mitochondrial tRNA and 16S-rRNA) in the CHIR-99021-treated and vehicle control-treated lean HLCs was determined by real-time PCR. n=3 different donors. (C) Protein levels of NDUFB8 and NDUFB9 in the CHIR-99021-treated and vehicle control-treated lean HLCs were determined by western blotting. Relative band densities of NDUFB8 and NDUFB9 were normalized to that of GAPDH and analysed using ImageJ software. n=3 different donors. Significance compared to the vehicle control. *N.S.*, not significant. Data are presented as the means ± SEM. lean HLCs, hepatocyte-like cells derived from adipose stem cell of lean donors; GAPDH, glyceraldehyde-3-phosphate dehydrogenase; NDUFB8, NADH: ubiquinone oxidoreductase subunit B8; NDUFB9, NADH: ubiquinone oxidoreductase subunit B9.

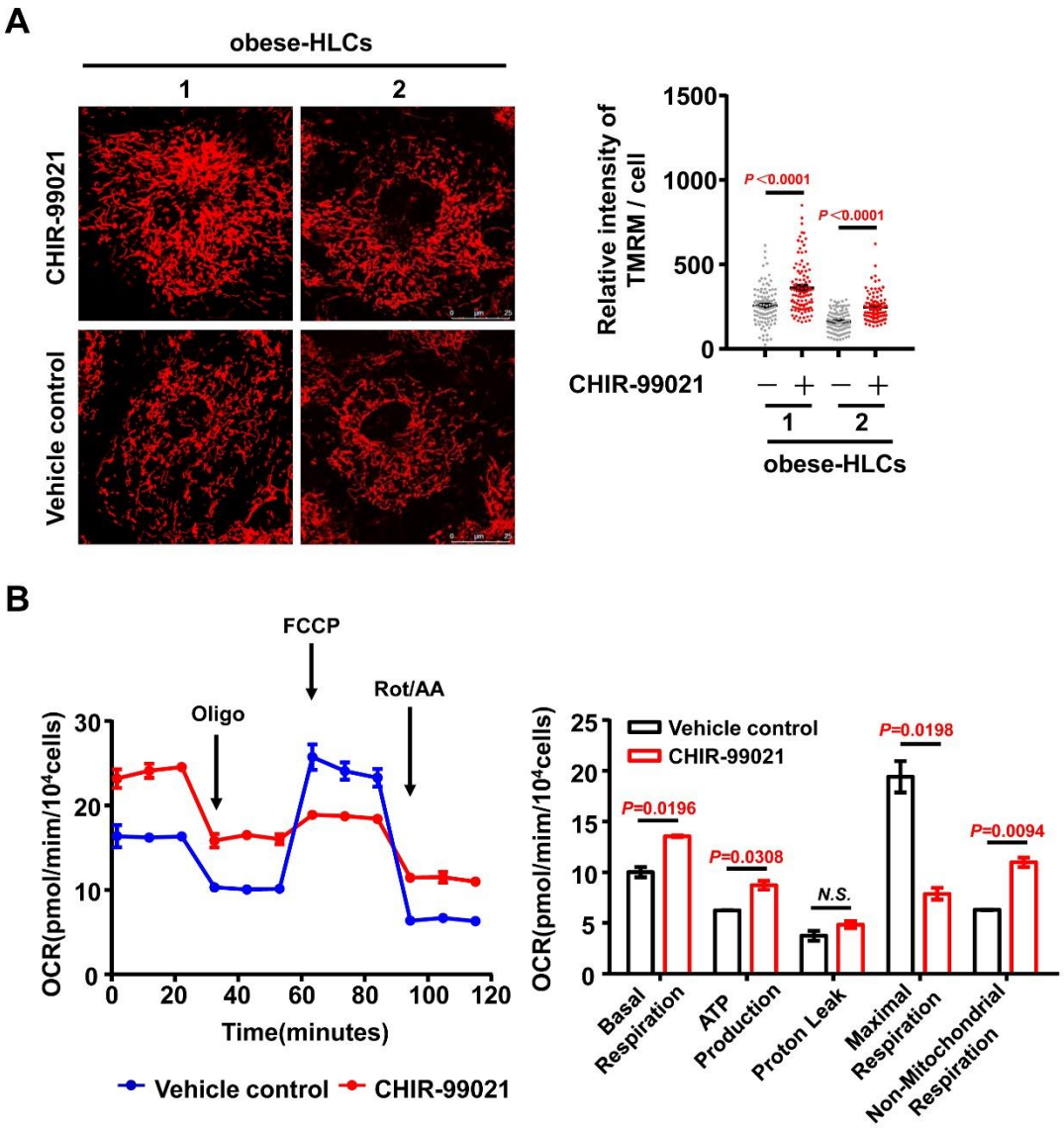

Figure S14. The mitochondrial function in the CHIR-99021-treated and vehicle control-treated obese HLCs was determined, Related to Figure 6. (A) Mitochondrial membrane potential in the CHIR-99021-treated and vehicle control-treated obese HLCs was determined by TMRM. Scale bars, 25 μm. The fluorescence intensity of TMRM in each cell was analysed using ImageJ software. n=2 different donors, the number of cells was 100 in each group respectively. (B) Kinetic profile of the OCR was measured in the CHIR-99021-treated and vehicle control-treated obese HLCs using a Seahorse XF Cell Mito Stress test. Black arrows show times of treatment with Oligo, FCCP, Rot and AA. The basal respiration, ATP production, proton leak, maximal respiration, and Non mitochondrial respiration were calculated. Significance compared to the vehicle control. *N.S.*, not significant. Data are presented as the means ± SEM. obese HLCs, hepatocyte-like cells derived from adipose stem cell of obese patients; OCR, oxygen consumption rate; Oligo, oligomycin; FCCP, carbonyl cyanide 4-trifluoromethoxy-phenylhydrazone; Rot: rotenone; AA, antimycin A.

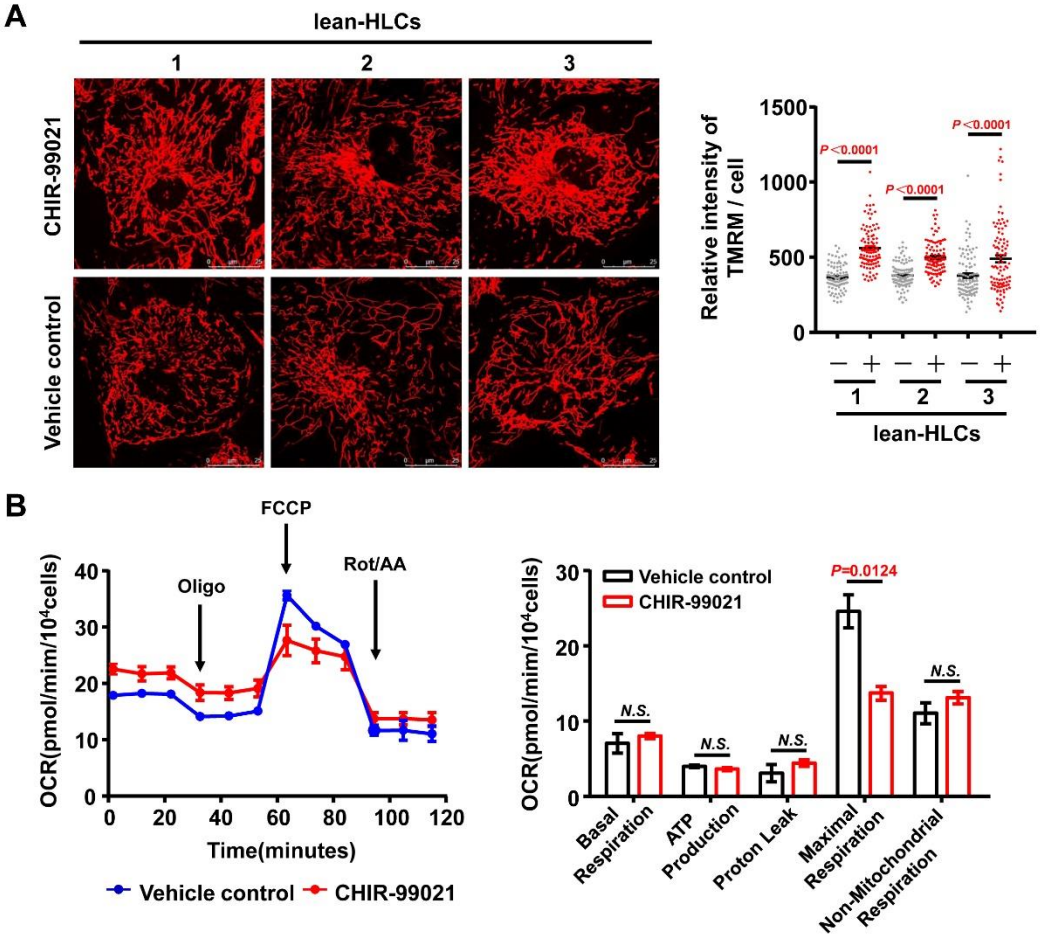

Figure S15. The mitochondrial function in the CHIR-99021-treated and vehicle control-treated lean HLCs was determined, Related to Figure 6. (A) Mitochondrial membrane potential in the CHIR-99021-treated and vehicle control-treated lean HLCs was determined by TMRM. Scale bars, 25 μm. The fluorescence intensity of TMRM in each cell was analysed using ImageJ software. n=3 different donors, the number of cells was 100 in each group respectively. (B) Kinetic profile of the OCR was measured in the CHIR-99021-treated and vehicle control-treated lean HLCs using a Seahorse XF Cell Mito Stress test. Black arrows show times of treatment with Oligo, FCCP, Rot and AA. The basal respiration, ATP production, proton leak, maximal respiration, and Non mitochondrial respiration were calculated. Significance compared to the vehicle control. *N.S.*, not significant. Data are presented as the means ± SEM. lean HLCs, hepatocyte-like cells derived from adipose stem cell of lean donors; OCR, oxygen consumption rate; Oligo, oligomycin; FCCP, carbonyl cyanide 4-trifluoromethoxy-phenylhydrazone; Rot: rotenone; AA, antimycin A.

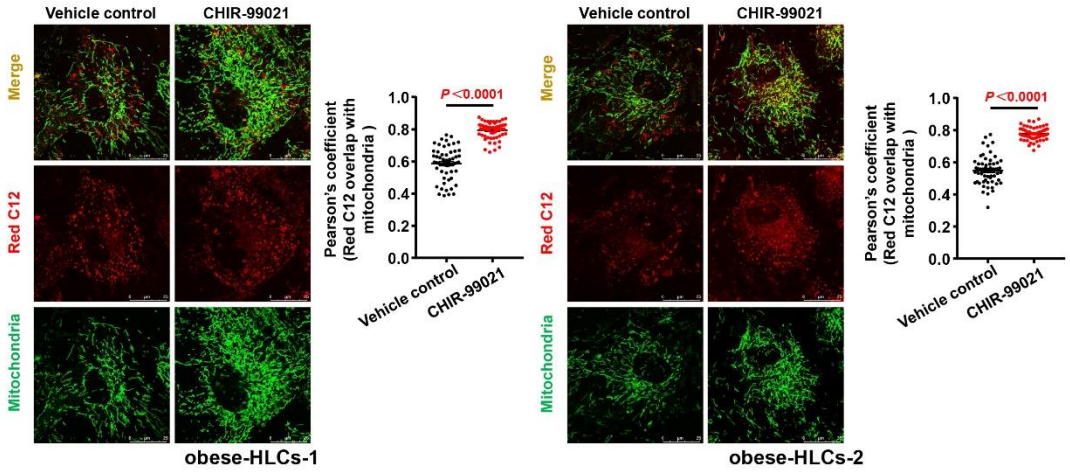

Figure S16. Fatty acid oxidation in the CHIR-99021-treated and vehicle control-treated obese HLCs was determined, Related to Figure 6. FAs were labeled using BODIPY 558/568 C_{12} (Red C12) and mitochondrial were labeled using MitoTracker Green FM. Scale bars, 25 μm. The fluorescent co-localization between Red C12 signal and mitochondria in the experiment was quantified by Pearson's coefficient analysis using ImageJ software. n=2 different donors, the number of cells was 60 in each group respectively. Significance compared to the vehicle control. Data are presented as the means ± SEM. obese HLCs, hepatocyte-like cells derived from adipose stem cell of obese patients.

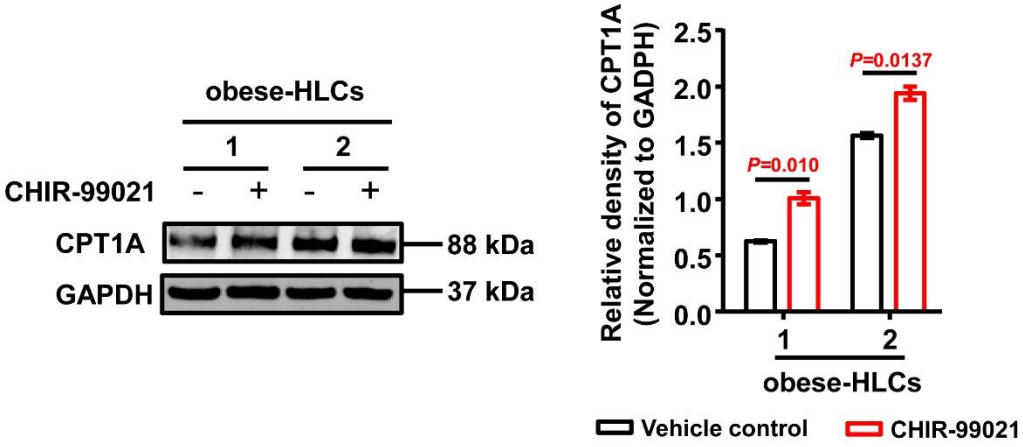

Figure S17. Protein levels of CPT1A in the CHIR-99021-treated and vehicle control-treated obese HLCs were determined by western blotting, Related to Figure 6. Relative band densities of CPT1A were normalized to that of GAPDH and analysed using ImageJ software. n=2 different donors. Significance compared to the vehicle control. Data are presented as the means ± SEM. obese HLCs, hepatocyte-like cells derived from adipose stem cell of obese patients; GAPDH, glyceraldehyde-3-phosphate dehydrogenase; CPT1A, carnitine palmitoyltransferase 1A.

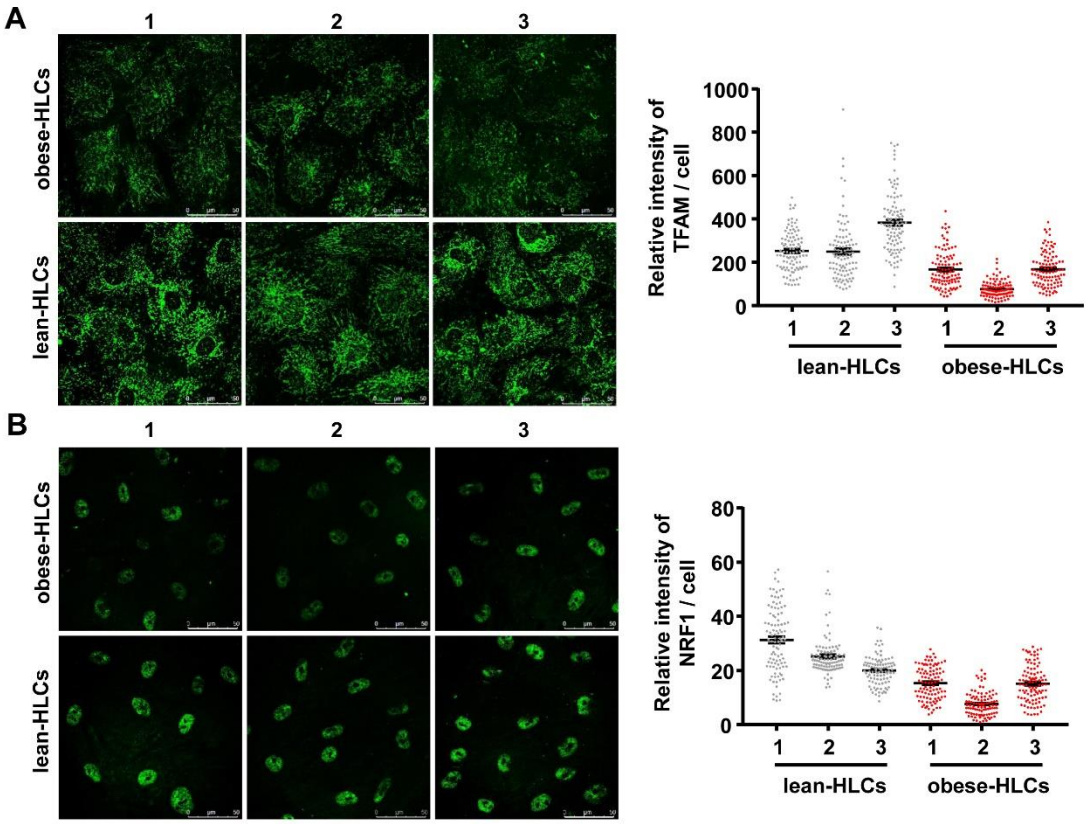

Figure S18. The relative protein levels of TFAM and NRF1 in the lean HLCs and obese HLCs were determined, Related to Figure 7. Relative immunofluorescence staining intensity of TFAM and NRF1 in each cell was analysed using ImageJ software. Scale bars, 50 μm. n=3 different donors per group, the number of cells was 100 in each donor respectively. Data are presented as the means ± SEM. lean HLCs, hepatocyte-like cells derived from adipose stem cell of lean donors; obese HLCs, hepatocyte-like cells derived from adipose stem cell of obese patients; TFAM, mitochondrial transcription factor A; NRF1, nuclear respiratory factor 1.

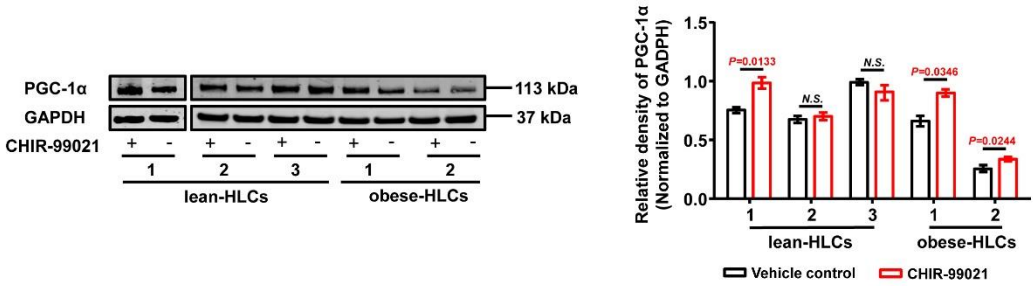

Figure S19. Protein levels of PGC-1α in the CHIR-99021-treated and vehicle control-treated lean or obese HLCs were determined, Related to Figure 7.

Relative band densities of PGC-1α were normalized to that of GAPDH and analysed using ImageJ software. n=2-3 different donors per group. Significance compared to the vehicle control. *N.S.*, not significant. Data are presented as the means ± SEM. lean HLCs, hepatocyte-like cells derived from adipose stem cell of lean donors; obese HLCs, hepatocyte-like cells derived from adipose stem cell of obese patients; GAPDH, glyceraldehyde-3-phosphate dehydrogenase; PGC-1α, peroxisome proliferator activated receptor gamma (PPARγ) coactivator 1 alpha.

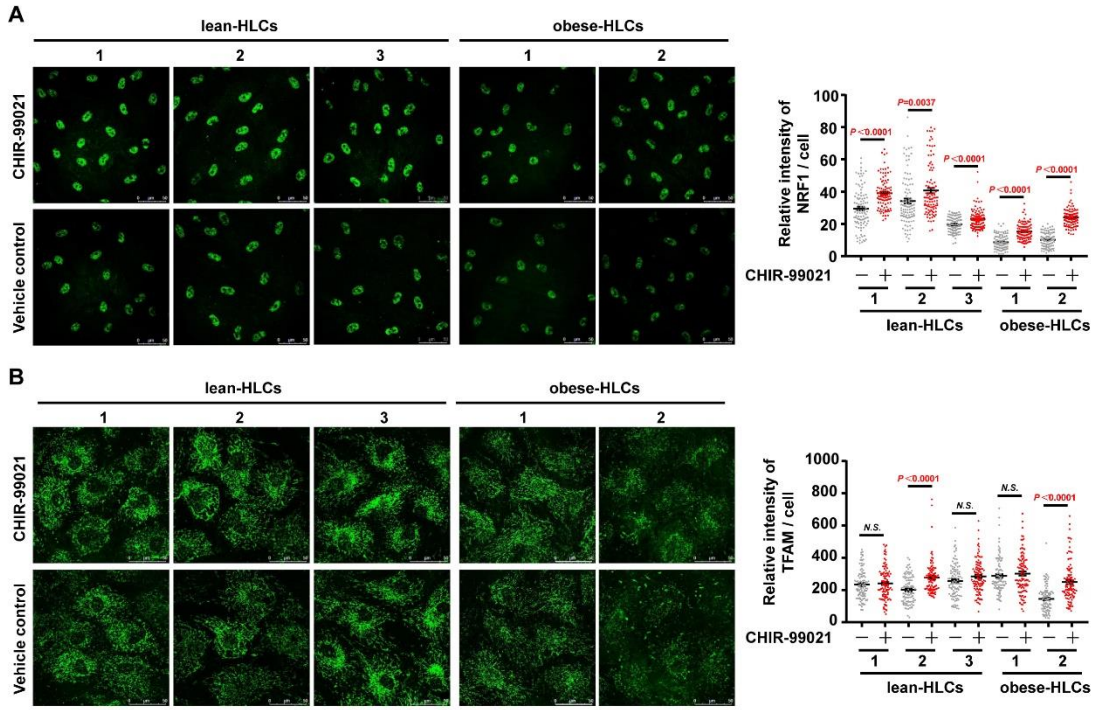

Figure S20. The relative protein levels of NRF1 and TFAM in the CHIR-99021-treated and vehicle control-treated lean or obese HLCs were determined, Related to Figure 7. Relative immunofluorescence staining intensity of NRF1 and TFAM in each cell was analysed using ImageJ software. Scale bars, 50 μm. n=2-3 different donors per group, the number of cells was 100 in each donor respectively. Significance compared to the vehicle control. *N.S.*, not significant. Data are presented as the means ± SEM. lean HLCs, hepatocyte-like cells derived from adipose stem cell of lean donors; obese HLCs, hepatocyte-like cells derived from adipose stem cell of obese patients; TFAM, mitochondrial transcription factor A; NRF1, nuclear respiratory factor 1.

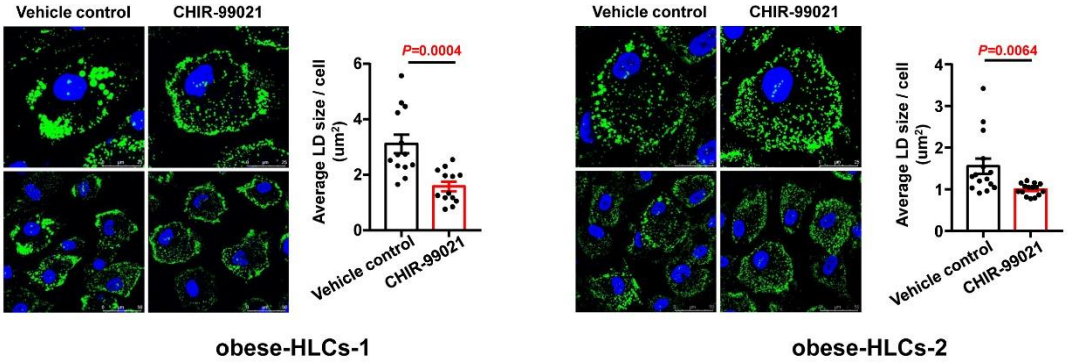

Figure S21. The LDs in obese HLCs were determined by HCS LipidTOX™ green neutral lipid staining, Related to Figure 8. Scale bars, 50 μm and 25 μm. The average size of LD in each cell was analysed using ImageJ software. n=2 different donors, the number of cells was 13 and 15 in each donor respectively. Data are presented as the means ± SEM. Significance compared to the vehicle control as analysed by unpaired two-tailed Student's t-test. obese HLCs, hepatocyte-like cells derived from adipose stem cell of obese patients; LDs, lipid droplets.

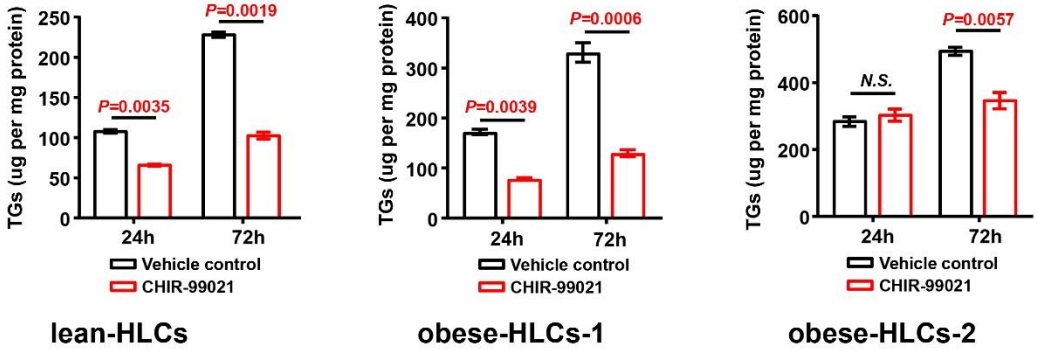

Figure S22. TG levels in the CHIR-99021-treated and vehicle control-treated lean or obese HLCs were determined, Related to Figure 8. Data are presented as the means ± SEM. Significance compared to the vehicle control as analysed by unpaired two-tailed Student's t-test. lean HLCs, hepatocyte-like cells derived from adipose stem cell of lean donors; obese HLCs, hepatocyte-like cells derived from adipose stem cell of obese patients.

Table S1. Summary of primer sequences used in the study，Related to Figure 1,3,4,5,7

Accession number	Name	5’-sequence-3’
NM_000477.7	ALB	F: CCCCAAGTGTCAACTCCAAC R: TCTTCTGCACAGGGCATTCT
NM_000392.5	ABCC2	F: AGCAGGTATTCGTTGGTT R: AGGTAGAGGCTTGGATTG
NM_001185039.2	ACOX1	F: GCCGCTATGATGGGAATGTG R: TTCGTGGACCTCTGCTTTGT
NM_014349.3	APOL3	F: CCTGTCTTTCCAGCATCCAC R: CTACAACCACCACCTCCACC
NM_001202855.3	CYP3A4	F: GGCGGATGTTGAAGTGAG R: GTTGGGTGTTGAGGATGG
NM_001122633.3	CPS1	F: AGCTATTACTGACCCTGCCTAC R: TGCTAAGTCCCAGTTCATCC
NM_001031847.2	CPT1A	F: TCCACGATTCCACTCTGCTC R: TACACGACGATGTGCTTGCT
NM_001025194.2	CES1	F: ACATGGTCGGAATTAACAAGC R: CCTCCTAAGTATTTCTCAGTGGC
XM_011523538.2	FASN	F: TCAAAGAAGCCCATCTCCCG R: CTGCTCCACGAACTCAAACACC
NM_013402.7	FADS1	F: CTGACTCAAACTCCTCCCTT R: CCTCTTCTGTTACCCTCCTG
NM_000167.5	GK	F: ATTTGGAGTTTGACAGGAGGAG R: TTCGCAGAGTTGTTTATCCC
NM_005110.4	GFPT2	F: CTCCACAGAACAGATCCCTATC R: GAGCTGTCCAGCCTCTTCAT
NM_000457.5	HNF4α	F: TTTTGGCTACTTGAGTTGTG R: CGTTCATTTCTGACCCTCT
NM_001098272.3	HMGCS1	F: AGCCACTTTCTGTCCTCTTG R: CCTGTTACCCTTGCTCTGTT
NM_000859.3	HMGCR	F: GAGATAGGAACGGTGGGTGG R: ATGTCCTGCTGCCAATGCTG
NM_001346590.1	INSIG1	F: CCCCATAGTGATTGAGTCTTC R: ATTCTCCACCTCCCTATTCT
NM_004139.5	LBP	F: TCGCCGACATTGATTATAGCT R: GGTAACTGGAGAACGGTGGT
NM_001317964.1	mt-tRNA (Leu)	F: CACCCAAGAACAGGGTTTGT R: TGGCCATGGGTATGTTGTTA
	mt-16S-rRNA	F: GCCTTCCCCCGTAAATGATA R: TTATGCGATTACCGGGCTCT
NM_001040110.1	NRF1	F: CAGCCGTCGGAGCACTTACT R: ACTGTTCCAATGTCACCACC

Accession number	Name	5’-sequence-3’
NM_001199987.1	NDUFB6	F: GTCCGTAGTTCGAGGGTGCG R: CCTTCAGCCATCGCCTTCTC
NM_001318195.2	NDUFA8	F: ATCCGAGGCGGTGTTTAGAG R: ACCCAGCCCAGTTTGTCCAG
NM_001284367.1	NDUFB8	F: AGTCCAGTGGCTGCAAAGGG R: ATCATCCGGGTAAGGTTCGT
NM_002496.4	NDUFS8	F: CATTGCCTGCAAGCTCTGCG R: GTCGATGTCATAGCGGGTGGT
NM_005002.5	NDUFA9	F: GGCTCACAGATTGTTCCTCC R: GTGCATCCGCTCCACTTTAT
NM_001278645.1	NDUFB9	F: CGTCAGCATCCACAGCCATAC R: TGGGACCTTGTAGCAATCGTATCT
NM_001018073.3	PCK2	F: ACCCTGCGAGTGCTTAGTGG R: AGTATTCTCAGCCTCAGTTCCATC
NM_001001928.3	PPARα	F: CCTGGTGACAGAACGAGACT R: CTACGCAAACCTGGAAATGG
NM_001311193.2	PLA2G4A	F: AGCTAGAGGCATTGAGGAGC R: CACTACCGTAAACTTGTGGG
NM_001330751.2	PGC-1α	F: TCCTTTCTCTCGCCCAACACGATCT R: GCATCCGACAGGACAAACAGTGGA
NM_001321099.2	PGAP1	F: TCCACTACCTACTCGCCAGAC R: TACCCTTGCTCAAACTACCTTC
NM_002592.2	PCNA	F: CGGTTACTGAGGGCGAGAAG R: TACAGGCAGGCGGGAAGGAG
NM_001316307.2	RAC3	F: GCACCCATCACCTACCCACAGG R: CGGATCGCCTCGTCAAACACT
NM_005063.5	SCD	F: TTGCGATATGCTGTGGTGCT R: ATAGGGAAAGGAGTGGTGGT
NM_001024956.2	SC5D	F: ACCCTATTGATGGCTTTCTT R: ATGGTGGTCTGTATGATGAG
NM_001270782.1	TFAM	F: TATTATGCTGGCAGAAGTCC R: CGCACAATAAAGAAACAACG
NM_000544.3	TAP2	F: TCCCAGGTAGGCTTTATGTC R: GGAGCAAACCAGGATTAGTG
NM_001068.3	TOP2B	F: CCGTCTTCAGATACAGTCCC R: ATCCGAGTCAGAGTTTACAGC
NR_003286.4	18S	F: GTAACCCGTTGAACCCCATT R: CCATCCAATCGGTAGTAGCG

Table S2. List of antibodies used in the study, Related to Figure 1,5,6,7

Primary Antibodies

Primary Antibody	Dilution	Company	Clonality	Cat. No.
Rabbit anti-AFP	1:200	Dako	polyclonal	A0008
Mouse anti-CD34	1:100	BD Biosciences	monoclonal	550761
Mouse anti-CD73	1:100	BD Biosciences	monoclonal	550257
Mouse anti-CD90	1:100	BD Biosciences	monoclonal	555595
Mouse anti-CD105	1:100	BD Biosciences	monoclonal	560839
Mouse anti-CPT1A	1:1000	Abcam	monoclonal	ab128568
Rabbit anti-GAPDH	1:1000	Cell Signaling Technology	monoclonal	5174
Rabbit anti-GATA4	1:100	Merck Millipore	polyclonal	AB4132
Rabbit anti-GSTA2	1:50	Abgent	polyclonal	AP9413α
Rabbit anti-NDUFB8	1:1000	Abcam	monoclonal	ab192878
Rabbit anti-NDUFB9	1:1000	Abcam	monoclonal	ab200198
Rabbit anti-NRF1	1:100	Abcam	monoclonal	ab175932
Rabbit anti-PGC-1α	1:1000	Abcam	monoclonal	ab188102
Rabbit anti-TFAM	1:100	Abcam	monoclonal	ab176558

Secondary Antibodies

Secondary Antibody	Dilution	Company	Clonality	Cat.No.
Alexa Fluor® 488 Conjugate (Goat Anti-Mouse IgG)	1:500	Cell Signaling Technology		4408S
Alexa Fluor® 488 Conjugate (Goat Anti-Rabbit IgG)	1:500	Cell Signaling Technology		4412S
IRDye 800CW Goat anti-rabbit (H+L)	1:10000	Abcam		ab216773

Transparent Methods

Ethics statement

All human visceral omental adipose tissues were obtained with donor consent, and experimental protocols were approved and carried out in accordance with the relevant guidelines and regulations of the Ethics Committee of Capital Medical University, China. All investigations were conducted according to the principles expressed in the Declaration of Helsinki.

Cell culture and differentiation

hASCs from lean donors (body mass index, BMI <24k/m^2) and obese donors (BMI >30 kg/m^2) were separately cultured and differentiated into HLCs, as described in our previous report (Li et al., 2014). Each group provided three to six different donors and cells from passages six to nine were used in this study. Once the hASC-HLCs were differentiated, these cells were harvested and seeded on the endothelial cell-derived matrix-coated substrate (Guo et al., 2017) at a density of 75,000/cm^2 with minimum essential medium with non-essential amino acids (MEM/NEAA; Invitrogen, Grand Island, NY), supplemented with 0.5 mg/ml bovine serum albumin (BSA; Sigma-Aldrich, St. Louis, MO, USA), 1% insulin-transferrin-sodium selenite (ITS; Sigma-Aldrich), 20 ng/ml hepatocyte growth factor (HGF; Peprotech, Rocky Hill, NJ, USA), 10 ng/ml oncostatin M (OSM; Peprotech) plus 10^{-6} M dexamethasone (DEX; Sigma-Aldrich). After a 6 hours incubation, the medium was changed to hepatocyte maintenance medium (Lonza, Walkersville, MD, USA), and cells were incubated overnight at 37°C with 5% CO_2. hASC-HLCs derived from obese patients were treated with or without CHIR-99021 (2 μM, Selleckchem, Houston, Texas, USA) for 24 hours.

Quantitative real-time RT-PCR

Quantitative real-time RT-PCR was performed as previously described (Guo et al., 2017). Total cellular RNA was extracted from 2.0×10^5cells with the RNeasy Mini Kit (QIAGEN, Hilden, Germany), according to the manufacturer's instructions. For PCR analysis, 0.5 μg of RNA was reverse-transcribed to cDNA using Superscript III reverse transcriptase and random hexamer primers (Invitrogen). Real-time PCR analysis was performed on a Thermo Fisher Scientific applied Biosystems QuantStudio 5 system (Applied Biosystems, Foster City, CA, USA) using the SYBR Green PCR Master Mix (Applied Biosystems). The reaction consisted of 10 μl of SYBR Green PCR Master Mix, 1 μl of a 5 μM mix of forward and reverse primers, 8 μl of water, and 1 μl of template cDNA in a total volume of 20 μl. Cycling was performed using the QuantStudio Design Analysis Software. The relative expression of each gene was normalized against 18S rRNA. The data are presented as the means ± SEM. The primers used are listed in supplementary materials Table S1.

Determination of mtDNA copy number

Total DNA from cells was obtained using the QIAamp DNA Mini Kit (QIAGEN). Quantitative real-time PCR was performed to quantify the mitochondrial DNA (mtDNA) content. Primers used for this experiment were specific to mt-tRNA (Leu) (Ma et al., 2019) , mt-16S-rRNA and the 18S rRNA unique gene sequences were used for the nuclear genomes. The primers used are listed in supplementary materials Table S1.

RNA sequencing and analysis

Approximately 1-2 μg of total RNA isolated from each independent biological sample was processed with NEB Next® Poly(A) mRNA Magnetic Isolation Module (New England Biolabs)

to mRNA enrichment. Sequencing libraries were then constructed using the KAPA Stranded RNA-Seq Library Prep kit (Illumina). The quality of the constructed sequencing libraries was analysed using an Agilent 2100 bioanalyser, and quantitative real-time PCR was performed to quantify the sequencing libraries. The mixed different sample libraries were sequenced using an Illumina HiSeq 4000 platform.

Image processing and base recognition were performed using Solexa pipeline software (version 1.8). The output sequencing read quality was analysed using FastQC software (version 0.11.7). The RNA-Seq reads were aligned to the human reference genome GRCh37 (also known as hg19) using HISAT2 (version 2.1.0) with default parameters. Only unique mapped reads were considered for further analysis. Gene expression was quantified using the FPKM (fragments per kilobase of transcript per million mapped reads) value. FPKM at the gene level and transcript level were calculated using Ballgown (version 2.8.4). A gene or transcript was considered expressed if its expression mean value is larger than or equal to 0.5 in each group. Differentially expressed genes with a fold change ≥1.5, *p*-value ≤ 0.05 and FPKM ≥0.5 were screened and retained in each group. The Gene Set Enrichment Analysis (GSEA) for Kyoto Encyclopedia of Genes and Genomes (KEGG) pathway and Gene Ontology (GO) analysis was analysed using GSEA (version 2.2.4).

The datasets generated and/or analysed during the current study are available in the GEO repository (GSE151760).

Immunofluorescence staining

For immunofluorescence analysis, the cells were fixed with 4% paraformaldehyde for 20 min at room temperature, followed by permeabilization with 0.3% Triton X-100 in phosphate buffered saline (PBS) for 5 min. The cells were rinsed and blocked with 10% goat serum (Zsgb-Bio, Beijing, China) for 60 min at room temperature. The cells were then incubated with the primary antibodies at 4°C overnight. Following three 5-min washes in PBS with gentle agitation, an Alexa Fluor-conjugated secondary antibody (Invitrogen) at 1:500 was added, and the samples were incubated for 1 h at 37°C. The nuclei were counter-stained with 4', 6-diamidino-2-phenylindole (DAPI, Sigma-Aldrich). The antibodies used are listed in supplementary materials Table S2.

Flow cytometry

For flow cytometric detection of surface antigens, hASCs (1×10^6 cells) were washed and resuspended in stain buffer (FBS) (BD Biosciences, San Jose, CA) containing saturating concentrations (1:100 dilution) of the following conjugated mouse monoclonal antibodies against human antigens (BD Biosciences) on ice for 30 min in the dark: endoglin (CD105)-PE, Thy-1 cell surface antigen (CD90)-FITC, CD34 molecule (CD34)-PE, and 5'-nucleotidase ecto (CD73)-PE. FITC labeled mouse IgG1κ Isotype control and PE labeled mouse IgG2ακ Isotype control were also included. The cell suspensions were washed twice and resuspended in FBS for flow cytometer (BD Accuri C6; BD Biosciences) using FLOWJO™ software (TreeStar, Inc., Ashland, OR). The antibodies used are listed in supplementary materials Table S2.

Mitochondrial labelling and imaging using live confocal fluorescence microscopy

Cells were seeded into confocal chambers (NEST Biotechnology, Wuxi, China) at a density of 50,000 cells per well. For mitochondria and nuclei staining, the cells were incubated with Hoechst 33342 (0.2 μg/ml, Thermo Fisher Scientific, Waltham, MA, USA) for 20 min at

37°C, then 50 nM MitoTracker Green FM (M7514, Thermo Fisher Scientific) or 25 nM TMRM (I34361, Thermo Fisher Scientific) was added. The cells were incubated for 30 min at 37°C and then washed three times with PBS. After washing, the images of fluorescently labelled mitochondria and nuclei were captured using a Leica TCS SP8 STED confocal laser scanning microscope (Leica, Wetzlar, Germany). The excitation/emission wavelengths for the individual dyes were 490/516 nm for MitoTracker Green FM and 548/574 nm for TMRM. The relative intensities of MitoTracker Green FM and TMRM were calculated in each cell was performed as previously described (Ma et al., 2019). The data are presented as the means ± SEM.

HCS LipidTOX™ green neutral lipid stain and analysis

Cells were fixed with 4% paraformaldehyde for 20 min at room temperature, and then washed three times with PBS. After washing, the cells were incubated with HCS LipidTOX™ neutral lipid stain (H34475, Invitrogen) diluted 1:1000 for at least 30 min at room temperature. The nuclei were counterstained with 4', 6-diamidino-2-phenylindole (DAPI, Sigma-Aldrich). The images of the fluorescently labelled lipid droplets and nuclei were captured using a Leica TCS SP8 STED confocal laser scanning microscope (Leica). The excitation/emission wavelengths for measuring HCS LipidTOX™ neutral lipid stain was 495/505 nm. Quantification of the LDs number per cell was performed using ImageJ software (National Institutes of Health, Bethesda, MD, USA). The data are presented as the means ± SEM.

Measurement of fatty acid oxidation and lipogenesis

For fatty acid and mitochondria staining, the cells were incubated with 50 nM MitoTracker Green FM (M7514, Thermo Fisher Scientific) for 30 min at 37°C, then 10 μM BODIPY 558/568 C_{12} (Red C12, D3835, Invitrogen) was added as previously described (Rambold et al., 2015). The cells were incubated for 40 min on ice in the dark and then washed three times with PBS.

For fatty acid and lipid droplets staining, the cells were incubated with 10 μM BODIPY 558/568 C_{12} (Red C12, D3835, Invitrogen) for 40 min on ice in the dark and then washed three times with PBS. After washing, the cells were fixed with 4% paraformaldehyde for 20 min at room temperature in the dark, and then washed three times with PBS. After washing, the cells were incubated with HCS LipidTOX™ neutral lipid stain (H34475, Invitrogen) diluted 1:1000 for at least 30 min at room temperature in the dark.

The images of fluorescently labelled fatty acid and mitochondria or lipid droplets were captured using a Leica TCS SP8 STED confocal laser scanning microscope (Leica). The excitation/emission wavelengths for the individual dyes were 558/568 nm for Red C12 and 490/516 nm for MitoTracker Green FM or 495/505 nm for HCS LipidTOX™ neutral lipid stain. Fluorescent co-localization of fatty acids and mitochondria represents fatty acid oxidation, fluorescent co-localization of fatty acids and lipid droplets represents lipogenesis in the experiment. The fluorescent co-localization between Red C12 signal and mitochondria or lipid droplets was quantified by Pearson's coefficient analysis using ImageJ'JACoP'software (National Institutes of Health). The data are presented as the means ± SEM.

Transmission electron microscopy analysis

The transmission electron microscopy (TEM) analysis was performed as previously described (Li et al., 2014). The samples were examined using a HT7700 transmission electron microscope (Hitachi, Tokyo, Japan).

Western blots

Cells were lysed on ice using a Nuclear and Cytoplasmic Extraction Reagent Kit (NE-

PER) (Thermo Fisher Scientific). The samples were normalized for protein concentration using the BCA protein assay. Each sample (8-10 µg) was analysed using 10% SDS-PAGE (Invitrogen) and transferred to a PVDF membrane (Merck Millipore, Darmstadt, Germany). The membranes were blocked in 5% BSA in TBST, and were incubated overnight at 4°C with the specific primary antibodies. Glyceraldehyde-phosphate dehydrogenase (GAPDH) was used as internal reference. The membranes were washed with TBST and incubated with IRDye-conjugated secondary antibodies for 1 h at room temperature. The membranes were scanned with the Odyssey detection system (Li-COR, Lincoln, NE, USA). Relative densities of proteins were quantitatively assessed using ImageJ software. The data are presented as the means ± SEM. The antibodies used are listed in supplementary materials Table S2.

Real-time ATP rate assay

The rate of ATP production simultaneously in live cells was detected as previously described using the Agilent Seahorse XF Real-Time ATP rate assay (Ma et al., 2019). The oxygen consumption rate (OCR) and extracellular acidification rate (ECAR) measurements were then assessed using a Seahorse XF Real-Time ATP Rate Assay Kit (Seahorse Bioscience, Billerica, MA, USA), according to the manufacturer's instructions. The ATP production rate, including the glycoATP production rate and the mitoATP production rate, was calculated using the Agilent Seahorse XF Real Time ATP Rate Assay Report Generator (Seahorse Bioscience). All measurements were normalized, and the three measurements of the basal (starting) level of the cellular OCR of each well were averaged. Each sample was measured in four wells. The experiments were repeated three times, with cells from three different donors per group.

Mitochondrial stress test

Mitochondrial function was detected in live cells using the Agilent Seahorse XF Cell Mito Stress Test Kit (Seahorse Bioscience). Briefly, hASC-HLCs were seeded on the endothelial cell-derived matrix matrix-coated 24-well XFe24 cell culture microplates with MEM/NEAA, supplemented with 0.5 mg/ml BSA, 1% ITS, 20 ng/ml HGF, 10 ng/ml OSM plus 10^{-6} M DEX , with 25,000 cells per well. After a 6 hours incubation, the medium was changed to hepatocyte maintenance medium (Lonza), and cells were incubated overnight at 37°C with 5% CO_2. Prior to measurements, cells were washed twice with warmed DMEM assay medium (XF assay-modified DMEM supplemented with 10 mM XF glucose, 1 mM XF pyruvate, 2 mM XF glutamine, pH 7.4) and incubated at 37°C in a non-CO_2 incubator for 45 min prior to the assay to allow cells to pre-equilibrate with the assay medium. The OCR and ECAR measurements were then assessed using a Seahorse XF Cell Mito Stress Test Kit (Seahorse Bioscience), according to the manufacturer's instructions, and using 1.0 µM oligomycin, 2.0 µM the uncoupler carbonyl cyanide 4-(trifluoromethoxy) phenylhydrazone (FCCP) and 0.5 µM rotenone/antimycin A. After measurement, the cell number per well was counted, and the OCR and ECAR measurements were normalized to the number of cells per well. The results were calculated using the Agilent Seahorse XF Mito Stress Test Report Generator (Seahorse Bioscience). All measurements were normalized. Each sample was measured in four wells. The experiments were repeated three times.

Measurement of mitochondrial reactive oxygen species content levels

The production of mitochondrial reactive oxygen species (ROS) was measured using MitoSOX™ mitochondrial superoxide indicator (M36008, Invitrogen). Briefly, hASC-HLCs

(1×10^6 cells) were resuspended in Hank's balanced salt solution (HBSS) buffer and incubated with a 5 μM MitoSOX™ reagent working solution for 15 min at 37°C in the dark. Next, the cells were washed three times and resuspended in HBSS buffer on ice in the dark. The levels of mitochondrial ROS were immediately measured by flow cytometry (BD Accuri C6; BD Biosciences), with excitation and emission spectra set at 510 nm and 580 nm, respectively.

Measurement of TG Content

TG levels were determined by using a triglyceride assay kit (Applygen Technologies, Beijing, China) following the manufacturer's instructions. Briefly, cells were incubated with lysis buffer for 10 min at room temperature and then heated for 10 min at 70°C, followed by centrifugation at 2000 rpm for 5 min at room temperature. The supernatants were analyzed according to the instructions with the EonTM Microplate Spectrophotometer (BioTek, Vermont, USA) at 550 nm. The total protein concentration was measured using the Pierce BCA Protein Assay Kit (Thermo Fisher Scientific) for normalization. The data are presented as microgram of TG per milligram of cellular protein.

Statistical analysis

All experiments were independently repeated more than three times with similar results. The statistical analyses were performed with GraphPad Prism 8 software using an unpaired two-tailed Student's *t*-test. The data are presented as the means ± SEM. At least three different donors per group. The differences were considered significant if $P<0.05$.

References

Guo, X., Li, W., Ma, M., Lu, X., and Zhang, H. (2017). Endothelial cell-derived matrix promotes the metabolic functional maturation of hepatocyte via integrin-Src signalling. J. Cell. Mol. Med. 21, 2809-2822.

Li, X., Yuan, J., Li, W., Liu, S., Hua, M., Lu, X., and Zhang, H. (2014). Direct differentiation of homogeneous human adipose stem cells into functional hepatocytes by mimicking liver embryogenesis. J. Cell Physiol. 229, 801-812.

Ma, Y., Ma, M., Sun, J., Li, W., Li, Y., Guo, X., and Zhang, H. (2019). CHIR-99021 regulates mitochondrial remodelling via beta-catenin signalling and miRNA expression during endodermal differentiation. J. Cell Sci. 132

Rambold, A.S., Cohen, S., and Lippincott-Schwartz, J. (2015). Fatty acid trafficking in starved cells: regulation by lipid droplet lipolysis, autophagy, and mitochondrial fusion dynamics. Dev. Cell. 32, 678-692.